Development of analytical methods and measurements of $^{13}C/^{12}C$ in atmospheric CH_4 from the NOAA/CMDL global air sampling network

John B. Miller[1,2], Kenneth A. Mack[2,3], Richard Dissly[1,4], James W. C. White[2,3], Edward J. Dlugokencky[1] and Pieter P. Tans[1]

1. NOAA Climate Monitoring and Diagnostics Laboratory, Boulder, Colorado
2. INSTAAR, University of Colorado, Boulder
3. Dept. of Geological Sciences, University of Colorado, Boulder
4. Present address: Blue Star Sustainable Technologies Corp., Arvada, CO

Abstract

We describe the development of an automated gas-chromatography isotope-ratio-mass-spectrometry (GC-IRMS) system capable of measuring the carbon isotopic composition of atmospheric methane ($\delta^{13}CH_4$) with a precision of better than 0.1 per mil. The system requires 200 mL of air and completes a single analysis in fifteen minutes. The combination of small sample size, fast analysis time and high precision has allowed us to measure background variations in atmospheric $\delta^{13}CH_4$ through the NOAA/CMDL Cooperative Air Sampling Network. We then present a record of $\delta^{13}CH_4$ obtained from six surface sites of the network between January 1998 and December 1999. The sites are Barrow, Alaska (71ºN), Niwot Ridge, Colorado (40ºN), Mauna Loa, HI (20ºN), American Samoa (14ºS), Cape Grim, Tasmania (41ºS) and the South Pole (90ºS). For the years 1998 and 1999, the globally averaged surface $\delta^{13}C$ value was -47.1 per mil, and the average difference between Barrow and the South Pole was 0.6 per mil. Consistent seasonal variations were seen only in the Northern Hemisphere, especially at Barrow where the average amplitude was 0.5 per mil. Seasonal variations in 1998, however, were evident at all sites, the cause of which is unknown. We also use a two-box model to examine the extent to which annual average $\delta^{13}C$ and CH_4 mole fraction measurements can constrain broad categories of source emissions. We find that the biggest sources of error are not the atmospheric $\delta^{13}C$ measurements but instead the radiocarbon derived fossil fuel emission estimates, rate coefficients for methane destruction, and isotopic ratios of source emissions.

1. Introduction

Atmospheric CH_4 is an important chemical component of both the stratosphere and troposphere and is a major contributor to the enhanced greenhouse effect. In the stratosphere, methane is a major source of water vapor [*Jones and Pyle,* 1984] and is the primary sink for chlorine radicals [*Cicerone and Oremland,* 1988], and thus plays an important role in the regulation of stratospheric ozone levels. In the troposphere, CH_4 consumes about 25% of all hydroxyl radicals, and as a result is an *in situ* source of CO and O_3 [*Thompson,* 1992]. Models indicate that the contribution of methane emissions to greenhouse warming is twenty times that of CO_2 on a per molecule basis [*Lashof and Ahuja,* 1990]. It is estimated that methane accounts for approximately 20% of the increase in radiative forcing by trace gases since the onset of the industrial era [*Myhre et al.,* 1998].

The amount of methane in the atmosphere has more than doubled in the last 150 years [*Etheridge et al.,* 1992; 1998] and over that time is highly correlated with human population [*Blunier et al.,* 1993]. The growth rate of methane in the atmosphere has averaged nearly 1% per year over the last 40 years [*Cicerone and Oremland,* 1988; *Etheridge et al.,* 1998] but has been steadily decreasing over the last 15 years [*Steele et al.,* 1992; *Dlugokencky et al.,* 1998]. Neither the rapid increase nor the recent slowdown is fully understood, and this is directly related to the large uncertainties in the magnitudes and spatial distribution of identified methane sources. Estimates of the emission rates of various sources are typically based upon small-scale field measurements [*Cicerone and Oremland,* 1988, and references within] that are extrapolated to large spatial scales. A few studies have used forward [*Fung et al.,* 1991] and inverse [*Brown,* 1993; *Hein et al.,*

1997; *Houweling et al.*, 1999] modeling approaches to estimate source distributions based on atmospheric measurements. Nonetheless, considerable uncertainties remain in the estimates of source strengths.

The measurement of the stable carbon isotope ratio in atmospheric methane [e.g., *Lowe et al.*, 1994; *Quay et al.*, 1999] and in methane sources [e.g., *Tyler*, 1986; *Conny and Currie*, 1996] may allow for a significant reduction in the uncertainties of the magnitudes of various methane sources. If we can measure $^{13}C/^{12}C$ of atmospheric methane with sufficient precision, and the kinetic fractionation associated with its consumption by the hydroxyl radical [*Cantrell et al.*, 1990] and soil microbes [*King et al.*, 1989], then we can determine the mass-weighted isotopic average of all methane sources at steady-state. When the mole fraction or $\delta^{13}C$ of CH_4 are not at steady-state, we also need to know their growth rates. If an isotopic "signature" can characterize different methane sources, then the mass-weighted average will be a constraint on the magnitudes of various methane sources. $^{13}C/^{12}C$ is commonly expressed as $\delta^{13}C$, which is defined as the part per thousand deviation of the $^{13}C/^{12}C$ ratio in a sample to that in a standard; *i.e.*, $\delta^{13}C \equiv [(R_{sample}/R_{reference})-1] \times 1000‰$, where $R=^{13}C/^{12}C$ and reference is V-PDB [*Craig*, 1957].

From a ^{13}C point of view, the sources of methane may be divided into three categories: bacterially produced methane, like that from wetlands or ruminants; fossil methane, like that associated with coal and natural gas deposits; and methane produced from biomass burning. Each of these three classes has a fairly distinct isotopic signature, with bacterial methane $\delta^{13}C \cong -60‰$, thermogenic methane $\delta^{13}C \cong -40‰$, and biomass burning methane $\delta^{13}C \cong -25‰$ [e.g., *Quay et al.*, 1999]. Individual methane sources

may differ significantly from their source type's characteristic signature, but the values above are averages that are probably valid on large spatial scales. In principle, we should be able to constrain the emissions from these three source types from global atmospheric measurements.

A few studies have reported globally and temporally distributed values of $\delta^{13}C$ in CH_4 [*Quay et al.*, 1991, 1999; *Stevens*, 1995]. Quay *et al.* [1999] reported more than 600 measurements between 1988 and 1995 from biweekly sampling at Barrow, AK, Olympic Peninsula, WA, Mauna Loa, HI, and American Samoa in addition to less frequent sampling at Cape Grim, Tasmania, and from Pacific Ocean ship transects. Stevens [1995] reported 201 measurements, mostly from the continental United States, between 1978 and 1989. $\delta^{13}C$ of methane in the Southern Hemisphere has also been regularly monitored at Baring Head, New Zealand since 1990 [*Lowe et al.*, 1994].

The goal of this study is to establish high-precision measurements of $\delta^{13}C$ of methane on a global basis, using a subset of sites in the NOAA/CMDL Cooperative Air Sampling Network [e.g., *Conway et al.*, 1994]. Since January 1998, we have measured $\delta^{13}C$ of methane from six sites (Table 1) ranging in latitude from 90 S to 71 N, from pairs of flasks collected on a weekly basis. The NOAA network gives us the potential to measure $\delta^{13}C$ of methane from more than 60 land and ship-based sites. In order to take advantage of the high temporal and spatial density offered by the network, we have designed an automated gas chromatography – isotope ratio mass spectrometry (GC-IRMS) system that analyzes samples using 200 mL of air in less than fifteen minutes. Traditional analysis methods [e.g., *Stevens and Rust*, 1982], on the other hand, are severely constrained by the 15 – 60 L of air typically used and the labor intensive sample

extraction and analysis. This paper describes the analysis system and presents data from the first two years of measurements.

2. Methods

Sample analysis can be separated into six steps: sample introduction, methane pre-concentration, cryo-focusing, chromatographic separation, combustion, and mass spectrometric analysis. The details of the reference air used, batch analysis and quality control will also be discussed below.

2.1 Sample Collection

Ambient air is pumped through a pair of serially connected 2.5 L glass flasks fitted with two glass-piston stopcocks sealed with Teflon O-rings. Conway *et al*. [1994] have described the collection method in detail. Whole air reference gas is collected in aluminum high-pressure cylinders at the NOAA/CMDL cooperative site at Niwot Ridge, Colorado, USA (40 N, 105 W, 3040m).

Samples are pressurized to roughly 0.2 bar above ambient pressure, resulting in 2.0 to 3.0 standard liters of air, depending on the altitude of the collection site. Upon arrival in Boulder flasks are analyzed for dry-air mole fractions of CH_4, CO_2, CO, H_2, N_2O, SF_6, and the carbon and oxygen isotopic composition of CO_2. On average, flasks contain less than 1.5 standard liters of air by the time they are analyzed for $^{13}C/^{12}C$ ratio of methane, which was a major constraint in the design of the analysis system. Air pressure in the flasks is also about 0.2 bar below ambient when extracted for measurement.

2.2 Sample Introduction

Flasks are attached to a manifold described in detail by Lang *et al.* [1990] in preparation for analysis. The circular manifold (Figure 1) is evacuated up to the flask stopcocks by a rotary pump (Edwards E2M5) to a pressure less than 3×10^{-2} mbar. The stopcocks on the flasks are then opened allowing the air inside to expand through tubing to an eight-port stream selection valve (Valco SD8, Valcon M rotor) fitted to a sixteen position electric actuator. These extra actuation positions allow the manifold to be in a "blanked off" position between the analyses of samples. A diaphragm pump (KNF) then pulls air out of the flask at rate of 100 mL/min (STP), controlled by an electronic mass flow controller (Edwards 1605). The air then flows through an Ascarite II (NaOH on a silica substrate) and $Mg(ClO_4)_2$ trap to remove CO_2 and water vapor from the sample. The CO_2/water trap is a 15 cm x 6 mm i.d. glass trap consisting of a six cm layer of Ascarite II sandwiched between two, 2 cm layers of $Mg(ClO_4)_2$, with small plugs of glass wool at each end. The Cajon Ultra-Torr fitting holding the trap on the downstream side also has a 10 μm stainless steel frit to prevent particles from entering the rest of the system. After leaving the trap, the air flows to a 40 mL sample loop positioned on a six-port, two-position injection valve (Valco 6-UW, Valcon E rotor). After flushing the sample loop and trap for 120 seconds, the injection valve is switched so that a flow of He (99.999 % purity, further purified by Alltech "All-Pure" He purifier) flushes the contents of the sample loop to another six-port, two-position valve containing the pre-concentrator (Figure 1). Note that the flowrate of the He stream is only pressure regulated resulting in changing flowrates with temperature and flowpath. The flowrates through the pre-concentrator are 22 mL/min (STP) at room temperature and 30 mL/min (STP) at –120 C.

The introduction of air from a reference tank has been designed to be as similar as possible to the introduction of flask air, so as to minimize any potential offset between analysis of reference air and sample air. The only difference is that reference air flows through the diaphragm pump while it is off. A downstream regulator pressure of at least 0.2 bar above ambient pressure on the reference air tank is needed to overcome the resistance of the water/CO_2 trap and maintain a flow of 100 mL/min (STP). A total of approximately 200 standard mL is used in each sample analysis. This volume is more than four times the volume of tubing that is flushed but decreases the chances that the trap contains any "memory" of the previous sample from run to run.

2.3 Sample Pre-concentration

Pre-concentration of the CH_4 within the air sample is necessary to ensure that N_2, O_2, and Ar do not co-elute with methane from the analytical column. N_2 entering the combustion furnace can be oxidized to N_2O, which interferes with the m/z = 44 and 45 signals that result from CH_4-derived CO_2. In general, we want only CH_4-derived CO_2 (and He) in the mass spectrometer during its analysis. The pre-concentration step is to isolate methane on a substrate while N_2, O_2, and Ar are vented. Our pre-concentrator is based on the design of Merritt *et al*. [1995] and modified to ease automation. The pre-concentrator is a linear 1/8" o.d. (0.085" i.d.) x 20 cm stainless steel column packed with 4 cm of 80/100 mesh Haysep-D surrounded by 5 cm of 60/80 mesh glass beads and 1 cm of glass wool on either side. The column is encased in a 12 cm x 6 mm i.d. glass tube, fitted with two 1/4" o.d. side-arms, as shown in Figure 2. A 1 cm thick insulating layer of open-cell foam covers the glass tube. The column is centered within the glass tube by a pair of 1/2" to 1/4" Cajon Ultra-Torr reducing unions through which the column

extends. The central 10 cm of the column is wrapped with fiberglass insulated NiCr heating wire (0.23 mm diameter, Omega). The wire is wrapped over a narrow gauge K-type (alumel/chromel, Omega) thermocouple positioned about 2 cm from the center of the column, just beside the liquid N_2 outlet (Figure 2). The column is fitted to the six-port, two-position valve with 1/16" stainless steel tubing and 1/16" to 1/8" reducing unions fitted with 10 μm screens (Valco) and sealed with Teflon ferrules.

The column is maintained at –120 C by opening and closing a solenoid valve on a pressurized liquid N_2 tank that is plumbed to the inlet of the jacket surrounding the pre-concentration column. The valve is controlled by the central computer, which monitors the thermocouple at a frequency of about 5 Hz. Cold N_2, mainly in the vapor phase, enters through one of the side-arms on the glass outer jacket and exhausts through the other side-arm and the gaps between the 1/8" o.d. column and the 1/4" ends of the Ultra-Torr fittings. Tests demonstrated that allowing liquid nitrogen to exhaust through the exit side-arm and both ends of the glass jackets provided the most uniform temperatures.

The pre-concentrator is kept at –120 ± 3 C for 3 minutes prior to the sample injection to ensure that the entire diameter of the column has cooled. Once the sample air has been injected onto the pre-concentrator, it is held at –120 C for 2 minutes allowing the bulk of the "air" to vent. Immediately after the cooling is stopped, the NiCr wire (total resistance = 19.7 Ω) is heated to 0 C by applying a 12 V potential across the NiCr wire. The central computer controls the warm temperature in the same manner as the cryogenic temperature. As soon as the heating begins, the six-port valve is switched so that the ~ 30 mL/min (STP) of He through the pre-concentrator is replaced by a 2.0 mL/min (STP) electronically controlled flow (Tylan FC-260). The low flow rate is

required by the analytical column and ensures a reasonable split ratio prior to entering the mass spectrometer. We chose 0 C to minimize the amount of water vapor released by the pre-concentrator on to the cryo-focus stage. After the elution of CH_4, the high He flow is returned to the pre-concentrator and it is heated to 110 C for 5 minutes to purge the column of H_2O and any other remaining condensables.

The temperatures and timings for the pre-concentrator were determined by analyzing both the venting flow and the slow eluting flow by Flame Ionization Detection (FID). At the measured temperature of –120 C methane was retained indefinitely on the pre-column. Although the FID is not directly sensitive to air, the flow disturbance caused by its elution is evident at about 15 seconds. The additional 105 seconds was used to let the tail elute. A column heating rate of about 40 C/minute, corresponding to an application of 12 V resulted in the elution of methane at 45 seconds after the valve switch and the start of heating, with a peak width (FWHM) of about 30 seconds. Tests using an NDIR analyzer (Li-Cor 6251) indicated that CO_2 co-elutes with methane in the absence of the pre-sample loop CO_2/H_2O trap.

2.4 Sample Cryo-focusing and separation

The methane eluting from the pre-concentrator is transferred to the GC through a 0.32 mm i.d. deactivated fused silica transfer capillary (SGE). There it is cryo-focused at the head of the analytical column (Molecular Sieve 5A, 0.32 mm x 25 m, Chrompack) so that its peak width can be reduced. The cryo-focusing is achieved by cooling the first 10 cm of the column to about –150 C. The head of the column is encased in a section of 1/4" o.d. stainless steel tubing with a tee at one end, and a cross at the other (Swagelok). The column is held in place by custom-drilled 1/4" – 0.5 mm graphitized–vespel reducing

ferrules. The tee is used as the inlet for liquid N_2 while the cross is used as an outlet and as a port for a K-type thermocouple. The central computer controls the temperature in the identical manner as the pre-concentrator. The head of the column is cooled one minute prior to the heating of the pre-concentrator to ensure that all eluting methane is trapped. It is held at –150 C for an additional 2 minutes, which corresponds to the FID - determined elution of methane from the pre-column plus one additional minute of "safety" time. The head of the column is heated by stopping the flow of liquid N_2 and simply allowing the cryo-focus device to warm to the GC temperature of 80 C. The column warms to 0 C within about 3 minutes, although design tests indicate methane begins to desorb from the column at about –100 C.

Methane and residual air from the pre-concentration step, along with air from leaks and carrier gas impurities are cryo-focused on the head of the analytical column. Some of this air passes through at –150 C, but the portion that is retained must be fully separated prior to combustion and analysis in the mass spectrometer. Although the dominant choice of analytical column in similar systems has been 0.32 mm x 25 m Poraplot Q [*Zeng et al.*, 1994; *Merritt et al.*, 1995; *Sansone et al.*, 1997], we have found that the separation of CH_4 from air is enhanced on Molecular Sieve 5A. At a GC oven temperature of 80 C, O_2 elutes at 100, N_2 at 150, and CH_4 at 190 seconds after the warming of the cryo-focus region. Furthermore, the strong retention of CH_4 on Molecular Sieve 5A allows for a much smaller length of column to be used in cryo-focusing.

The GC effluent prior to the elution of CH_4 is diverted from the source of the mass spectrometer through a change-over valve located downstream of the open-split

(Figure 1). The wide separation ensures that when CH_4 is present in the combustion furnace and the analyzer section of the mass spectrometer, no other species (other than He carrier gas) are present. The width (FWHM) of the methane peak after conversion to CO_2 is five seconds as measured by the mass spectrometer. The peak height is typically about 9 nA (Figure 3) but can vary depending upon both the sensitivity of the mass spectrometer and the temperature of the cryo-focus unit. CO elutes at 350 seconds, but the ratio of its peak area to that of methane indicates that only a portion of the initial CO in the sample is trapped during methane pre-concentration. Although the Molecular Sieve column has excellent separating characteristics, it irreversibly adsorbs water and CO_2 at room temperature. The presence of the trap upstream of the sample loop prevents the majority of water and CO_2 from reaching the column, but the column must be baked out after every ~500 samples at greater than 200 C to remove adsorbed water and CO_2.

2.5 Sample Combustion

After eluting from the capillary column the methane peak is transferred to the combustion furnace via a 20 cm section of 0.32 mm i.d. fused silica capillary. The combustion furnace is composed of a 3 mm o.d. x 0.5 mm i.d. x 300 mm high-density alumina tube (Alsint, Bolt Technical Ceramics) mounted co-axially within a 400 W cylindrical heater. The combustion tube is attached to transfer capillaries on either end by 1/8" – 1/16" reducing unions (Valco), and the seal is made with 1/8" graphitized-vespel ferrules and 1/16" gold-plated stainless steel ferrules (Valco). The output of the heater is controlled by an electronic temperature controller (Omega 9000A) using an R-type (Platinum and Rhodium/Platinum, Omega) thermocouple. The ceramic tube extends 6 cm beyond the edges of the heater to ensure that the fittings remain cool. Glass wool is

used to plug both ends of the annulus between the combustion tube and the heater to minimize the temperature gradient within the heated zone.

The combustion tube is filled with Ni and Pt wires that run the length of the furnace. The Ni wire is used as a substrate for oxygen required in combustion, and the Pt wire serves as a catalyst. In order to maximize the amount of oxygen available for combustion and the surface area available for catalysis, six 0.05 mm Ni (99.994% purity) and two 0.05 mm Pt wires (99.95 % purity) are used (Alfa Aesar). All wires were braided together to facilitate insertion. The furnace is maintained at 1150 C; lower temperatures allow some methane to remain uncombusted. The Ni inside the furnace was initially oxidized by passing pure oxygen (99.999% purity) through the furnace at 5 mL/min (STP) at 500 C for 4-6 hours, and then at 1150 C for 10-12 hours [*Merritt et al.*, 1995]. However, repeated oxidation is not necessary. This is, most likely, because of the small amount of oxygen eluting through the column and passing into the furnace every time a sample is analyzed. The increased surface area of Ni wire, compared to that of Merritt *et al.*[1995], may also provide a larger reservoir of oxygen available for combustion. This design yields a consistent amount of CO_2, no CH_4 and no CO, as measured by the mass spectrometer, FID, and reduction gas analyzer, respectively. Based on these tests we infer a combustion efficiency of 100%.

Although water is produced in the combustion of methane, it is not removed from the He stream prior to admittance to the mass spectrometer. Normally, transient amounts of water are removed to limit the extent of the gas-phase ion-molecule reaction between CO_2 and H^+ in the source of the mass spectrometer. In this reaction, a proton bonds to the CO_2 resulting in a species of m/z = 45 that does not correspond to CO_2 containing

^{13}C. This reaction occurs in all IRMS's, but is "invisible" when its contribution is the same for both running gas and sample gas. In our case the rate of this reaction is substantially higher when our CH_4-derived CO_2 peak enters the source than when our pure CO_2 running gas does, resulting in a systematic error to our measurements. Such systematic errors can be accounted for by calibration. However, random variations in the H_2O peak and drifts in the background concentration of H_2O in the source over time do contribute to imprecision in our measurements. Fortunately, as shown below, these random errors are small.

2.6 Mass spectrometric analysis

After the CH_4-derived CO_2 peak leaves the combustion furnace it is transferred to an open split. The split consists of a 0.11 mm i.d. capillary placed 4 cm within a 0.32 mm i.d. capillary that is bathed in He. A 1 m section of the 0.11 mm capillary leads through the change-over valve to the source region of the mass spectrometer (Micromass Optima or Micromass Isoprime), resulting in a pressure of $5 – 6 \times 10^{-6}$ mbar. The split ratio is approximately 1:6. Although a larger split ratio would allow more CH_4-derived CO_2 to be analyzed, the mass spectrometer cannot operate at pressures greater than 1×10^{-5} mbar.

Inside the mass spectrometer, the CH_4-derived CO_2 is ionized and the signals for m/z = 44, 45, and 46 are simultaneously measured. After the tail of that peak has disappeared, after about one minute, a pulse of pure CO_2 "running gas" ("bone-dry" quality) from the bellows of the dual-inlet portion of the mass spectrometer is mixed into the He stream and admitted to the source region (Figure 1). The purpose of the pure CO_2 running gas is to track and correct for changes in the mass spectrometer ion source that

occur over periods of half an hour to hours. This square peak of CO_2 is thirty seconds wide with a height of about 6 nA. The CO-derived CO_2 peak elutes about 20 seconds after the end of the running gas CO_2 peak. Once the baseline has returned to normal after another 60 s, the signal collection is stopped.

Each aliquot of air, from either a sample flask or reference tank is measured relative to running gas, so that drifts in the source or analyzer regions of the mass spectrometer at time scales of greater than a few minutes are taken into account. Specifically, the m/z = 44, 45, and 46 peaks are integrated for both the sample and running gas, and ratios of the areas are calculated. The data analysis software measures the current at the beginning and end of the data collection period, linearly interpolates between those points, and subtracts these "zero" lines from the raw signals. The m/z= 44, 45, and 46 peaks have slightly different elution times, requiring each peak to have unique integration limits. The software makes an "isotope-shift" correction to the m/z = 45 and 46 peaks that are typically –40 ms and +20 ms, respectively. In order to correct for the contribution of $^{12}C^{16}O^{17}O$ to the m/z = 45 signal, a "Craig Correction" is made [*Craig*, 1957] based on the area of the m/z=46 peak. Finally, the $\delta^{13}C$ value of the sample peak is calculated relative to that of the running gas, and then converted to the V-PDB scale using the user-entered V-PDB value of the running gas.

The $\delta^{13}C$ value of our running gas relative to V-PDB is –36.9‰ as determined on a dual inlet instrument (Micromass – Optima) in our lab. However, we cannot be certain that this is the $\delta^{13}C$ value that is admitted to the source. The running gas is probably fractionated in the stainless steel capillaries between the bellows and the mass spectrometer, and the degree of fractionation can vary with the pressure in the bellows.

In addition, it is possible that fractionation can occur in the introduction of running gas to the bellows from our CO_2 source, and through leaks in the dual inlet of the mass spectrometer. Other day-to-day variability may result from changing baseline conditions and their effect on zero – subtraction. The consequence of these errors is that at this point the calculated delta values of both our samples and references differ from their true values by $+1.0 \pm 0.2$ ‰, on average.

2.7 Reference gases and calibration

In order to know the "true" value of our samples and references, our references have been externally calibrated using traditional, dual-inlet, off-line techniques. Four references have been calibrated by Dr. Stanley Tyler at the University of California, Irvine using a technique based on that of Stevens and Rust [1982; *Tyler*, 1986; *Lowe et al.*, 1991]. The $\delta^{13}CH_4$ of the reference air was measured relative to pure CO_2 reference gas that had been calibrated against IAEA-NZCH [see e.g. *Lowe et al.*, 1999]. The isotopic compositions of our samples and one additional reference air tank have been determined relative to these calibrated references. Our reference air is whole air that has been dried by $Mg(ClO_4)_2$ and pumped into aluminum cylinders to about 150 bar at Niwot Ridge, CO. In the future, at least one of our original reference air tanks will be re-measured by the Tyler group to check for drift in the $\delta^{13}C$ value. All measurements are reported relative to V-PDB [*Coplen*, 1995].

2.8 Analysis Sequence

Each sample flask is measured as part of a batch of eight. The run starts with the analysis of five consecutive aliquots of reference air, of which the first is typically an outlier (greater than 2σ from the mean), and always rejected. The measurement of the

flask samples then begins, and each sample analysis is alternated with a reference analysis until all eight samples have been measured. The batch analysis ends with the measurement of four consecutive aliquots of reference gas. Once the first reference measurement has been excluded, the reference measurements are averaged in three groups of five, i.e. run #'s 2,3,4,5 and 7; 9,11,13,15 and 17; and 19,21,22,23,24. In this way, the drift of the total system over times of about two hours is tracked. Reference gas and sample gas are alternately introduced to the system to reduce the chances of "memory" of a previous sample affecting future samples. Standard gas $\delta^{13}C$ values are linearly interpolated between the averages of groups 1, 2, and 3. Flask sample $\delta^{13}C$ values are then re-calculated relative to the interpolated standard gas values to correct for drift. Drifts of about 0.1‰ are typically observed between the beginning and end of a run (about 6 hours), with the ending standard gas $\delta^{13}C$ values heavier than those at the start. One possible explanation for this drift is the accumulation of water vapor in the source region of the mass spectrometer over the course of the run. Water produced as a result of methane combustion and admitted through leaks may not be pumped away from the tubing downstream of the furnace, and the source, as fast as it is produced. From one sample/standard analysis to the next, this effect would be difficult to observe, but over the six hour period of the run, we would expect to observe some accumulation. Regardless of the cause of the drift, our frequent use of reference gas gives us confidence in the accuracy of our measurements relative to that of the externally calibrated reference air.

2.9 Quality Control

2.9.1 Flask Tests

In order to quantify systematic biases in the measurement of air from under-pressure flasks versus that from over-pressure tanks, we conducted systematic flask tests. Eight flasks were filled from a tank of standard gas to about 0.5 bar, which is the typical pressure in flasks when they are analyzed. The $\delta^{13}C$ values of these flasks were measured, in the manner stated above, and compared to the $\delta^{13}C$ values of the standard aliquots of the same batch analysis. Analysis was repeated twice more on these flasks to simulate three total measurements. No systematic bias was detected within the noise ($1\sigma \cong 0.05$ ‰) to which all samples and standards were subject. Additionally, the $\delta^{13}C$ values of the flasks from the first and third runs were not distinguishable, implying that we can analyze a flask at least three times without error.

2.9.2 Flask Pair Differences

One measure of the precision of flask analyses is the difference between the $\delta^{13}C$ values of a single flask and its mate. The mean pair difference is –0.018‰ (first flask measured minus the second), and the mean of the absolute values of pair differences is 0.118‰ (n=630). The distribution of pair differences is well approximated by a normal distribution centered on zero (Figure 4), indicating that there is no systematic bias in the order in which a pair of flasks is measured. Among good pairs, defined as those pairs with a difference less than 0.2‰, the mean pair difference is –0.009‰ and the mean absolute difference is 0.071‰ (n=554).

2.9.3 Precision of Standards

We can also use the standard deviation of the standards in a batch analysis as a proxy for the precision of flask measurements. The mean standard deviation of aliquots from standards in any given run is 0.08‰ ± 0.02‰ (1σ, n= 172) (Figure 5). Since all measurements are corrected for the drift of standards during a run, we also calculate the absolute difference between the measured $\delta^{13}C$ value and the $\delta^{13}C$ value of the linearly interpolated drift line, at the same point in time. The standard deviation of these differences is 0.07‰ ± 0.02‰. Using a 40 mL air sample, the shot-noise limited precision of our measurement is ~ 0.02‰, so we are within a factor of four of this limit.

2.9.4 Sample size v. d ^{13}C relationship -- "Linearity"

The relationship between sample size and $\delta^{13}C$ value was checked by making repeated measurements from a single standard tank using 40 mL and 25 mL sample loops. Although peak area as measured by the mass spectrometer varied in proportion to sample loop size, the $\delta^{13}C$ value was constant to within typical experimental uncertainty of ~0.05‰. Given that the mole fraction of methane in sample flasks varies by a maximum of ±15%, we are confident that "non-linear" effects in the chromatographic/combustion system or ion source do not compromise our measurements.

2.9.5 Internal Comparison of Reference Tanks

We have measured the $\delta^{13}CH_4$ values of our standard tanks relative to one another and compared the measured differences to the differences between tanks as originally measured at UCI. Since the $\delta^{13}C$ values encompass a range from –47.17 to –47.27‰, we measured only the two tanks at the ends of the scale. These two tanks are also the tanks that have provided the standard gas for close to 90% of our sample measurements.

Treating the tank "Harpo" as the standard and the tank "Lucy" as an unknown, the $\delta^{13}C$ value of Lucy was determined to be –47.14±0.01‰ (standard error of the mean, n=16), whereas the assigned $\delta^{13}C$ value of "Lucy" as determined at UCI is –47.17±0.04‰ (standard deviation, n=2).

2.9.6 Contamination levels

We intermittently assess the level of contamination in our analysis system by injecting a sample loop filled with He instead of air. Such blank runs never yield CH_4-derrived CO_2 peak areas of greater than 0.1% of the sample peak area. As an alternative test, we inject a He filled sample loop into the system but bypass the pre-concentration device. These tests yield peak areas only 0.03% of sample peak area. Thus, the contamination that is present is mostly due to condensation of leaks and carrier gas impurities during sample pre-concentration.

2.10 Future measurements of D/H

The system described above is well-suited for adaptation to make measurements of δD in atmospheric methane. The oxidation furnace currently in line could be replaced by a furnace that would directly convert CH_4 to H_2 [*Burgoyne and Hayes*, 1998; *Hilkert et al.*, 1999]. The hydrogen isotopic ratio could then be analyzed by an isotope ratio mass spectrometer appropriately tuned. The other change that would have to made would be to increase the size of the sample loop to account for the lower relative abundance of D compared to ^{13}C and the lower ionization efficiency of H_2 relative to CO_2. Assuming a CH_4 to H_2 conversion efficiency of near 100% and using a 100 mL sample loop, precision close to 1‰ should be attainable.

3. Results and Discussion

3.1. Editing and Selection of Data

Sample data are shown in Figure 6. Most data are averages of a single aliquot taken from each member of a pair of flasks, and less than 1% of the data are from unpaired flasks. At some sites samples are collected by different methods on the same day. The observed variations in the value of $\delta^{13}C$ are a composite of large and small-scale spatial variations, sampling errors, and analytical errors. Following the convention of *Dlugokencky et al.* [1994], data are first "edited" for sampling and analytical problems. Methane data exclusion on the basis of sampling and analytical problems has been discussed previously [*Lang et al.*, 1990; *Dlugokencky et al.*, 1994], but can involve problems associated with incomplete flushing of sample flasks and obvious contamination from local sources. Data are then edited for analytical problems that occurred during methane mole fraction measurements. Any sample determined to have either a problem in sampling or in the analysis of methane mole fraction is similarly flagged in the $\delta^{13}C$ data set. Samples analyzed during batch analyses where the standard deviation of the standard gas aliquots exceeded 0.12‰ are also flagged. Samples from these analyses are typically re-run. Data are also flagged and excluded from further analysis if the difference in $\delta^{13}C$ values from a flask pair exceeds 0.2‰. Pair differences greater than 0.2‰ most likely indicate analytical problems and not natural variability. Note that all data, including those flagged for sampling and analytical problems are available at ftp://www.cmdl.noaa.gov.

After editing, data are "selected" to ensure that they are representative of a very large volume of well-mixed air. Air samples determined to be "non-background" on the

basis of the methane mole fraction, as described by *Dlugokencky et al.* [1994], are flagged as such in the $\delta^{13}C$ data set. Air samples are also be determined to be "non-background" if the $\delta^{13}C$ value lies beyond a 3σ window around the smooth curve (see section 3.3) shown in Figure 6. Most often, a sample is considered background if it was collected when winds were coming from a pre-determined clean-air sector. In the first two years of data 2% of samples were excluded because of sampling problems and mole fraction analysis problems, 12% of the data were excluded because of $\delta^{13}C$ analysis problems and 2% were determined to be "non-background" on the basis of $\delta^{13}C$ value.

3.2. Latitudinal Gradient of $d^{13}C$

The north-south gradients in methane mole fraction and its isotopic composition are important constraints on the location and strength of methane sources and sinks [*Fung et al.*, 1991]. The mole fraction latitudinal gradient is well established [e.g., *Steele et al.*, 1987; *Dlugokencky et al.*, 1994], and Quay *et al*.[1991, 1999] have reported an annual mean gradient for $\delta^{13}C$. Figure 7 shows the annual mean gradients for 1998 and 1999 between 90 S and 71 N. The average difference between SPO and BRW (BRW – SPO) was -0.65 ± 0.1‰ in 1998 and –0.56 ± 0.1‰ in 1999. Quay *et al.* [1991] reported a mean annual average difference of -0.54±0.05‰ between BRW (71 N) and CGO (41 S) during the years 1989 - 1995. We calculate the annual mean hemispheric difference by fitting a cubic curve to the latitudinal profile, as a function of sine of latitude, and take the average δ value north and south of the equator. For the period 1998-1999 the mean hemispheric difference was 0.30 ‰.

As expected, the $\delta^{13}C$ values in the Southern Hemisphere are consistently higher than $\delta^{13}C$ values in the Northern Hemisphere. This occurs because the majority of

sources are located in the Northern Hemisphere, and the reaction with OH enriches the methane remaining in the atmosphere. Methane in the Southern Hemisphere has had more time to react with OH than methane in the Northern Hemisphere, leaving it more enriched in the heavy isotope. Another prominent feature of the inter-hemispheric gradient is the near uniformity of Southern Hemisphere $\delta^{13}C$ values. This is also observed in the inter-hemispheric gradient of methane mole fraction and is a function of paucity of surface emissions and rapid atmospheric mixing in the Southern Hemisphere [*Law et al.*, 1992].

3.3. Seasonal Variations in $\delta^{13}C$

Figure 8 shows monthly mean $\delta^{13}C$ values and mole fractions for the triad of sites in each hemisphere. Monthly mean $\delta^{13}C$ values are calculated from the smooth curves shown in Figure 6. The smooth curve for each site is represented by a function composed of a linear term to represent the long-term trend in the data and four harmonic terms, which capture the average seasonal variation.

$$f(t) = a_1 + a_2 t + \sum_{i=1-4} [a_{2i+2} \sin(2\pi i t) + a_{2i+3} \cos(2\pi i t)] \qquad (1)$$

The function is fit to the data using a least squares technique, which has been described in detail previously [*Thoning et al.*, 1989; *Steele et al.*, 1992; *Dlugokencky et al.*, 1994]. We average monthly portions of the smooth curve to give monthly mean $\delta^{13}C$ values, because the data are not evenly spaced. Samples are not collected every week, and sampling problems or non-background conditions may occur at a site during a given month. Monthly mean values remove some of the short-term natural variability and analytical variability in the data and allow for a more straightforward comparison to the mole fraction data.

3.3.1. Southern Hemisphere Sites

In our record, Southern Hemisphere sites SPO (90 S), CGO (41 S), and SMO (14 S) do not exhibit strong seasonal variability. During 1998, however, substantial decreases in monthly mean $\delta^{13}C$ values are present during August, September and October, especially at SMO and CGO. The conventional assumption is that seasonal variations in SH mole fractions are driven mostly by OH oxidation, but the magnitude of the dip in $\delta^{13}C$ values is too large to be explained by OH alone. One possible contribution to the observed dip is the positive 12 Tg/yr anomaly in tropical wetland emissions during 1998 proposed by *Dlugokencky et al.* [*Dlugokencky et al.*, 2001]. A +12 Tg/yr anomaly would result in a -0.13‰ anomaly in the lower Southern atmosphere (0-30ºS) if the emissions mixed evenly through the entire semi-hemisphere and if the signature of the wetland source were –60‰. The seasonal cycle amplitudes at CGO, based on the smooth curve fit to the data, were 0.26‰ in 1998 and 0.12‰ in 1999. Thus, anomalously large tropical wetland emission could help to explain the presence of the dip at SMO and CGO in 1998.

Lowe *et al.* [1997] showed distinct seasonal cycles in $\delta^{13}C$ between 1989 and 1997 from air collected at Baring Head. As discussed by Lowe *et al.* [1994], the amplitude of the observed seasonal cycle was too large to be explained solely on the basis of OH oxidation. If the methane mole fraction seasonal amplitude were controlled completely by OH destruction (as might be the case for SPO), we would expect the amplitude in $\delta^{13}C$ value to be approximately 0.1 ‰ according to the following Rayleigh model of CH_4 consumption.

$$\delta - \delta_o \approx -\varepsilon \frac{\Delta M}{M} \qquad (2)$$

Here, δ and δ_0 are the original, and final isotopic ratios, expressed in δ-notation (‰ units), ε is the kinetic fraction factor due to reaction with OH (ε=-5.4‰ [*Cantrell et al.*, 1990]) and $\Delta M/M$ is the fraction of total methane destroyed ($\Delta M/M$ = 30 ppb/1700 ppb). Given the analytical noise in our measurements of ~ 0.1‰, we may not be able to clearly observe a seasonal cycle with an amplitude of the same order. However, the Lowe *et al.* [1997] measurements indicate the presence of a seasonal cycle with an amplitude of at least 0.2‰. It is unclear at this point in our measurement record whether or not we are observing a seasonal cycle in $\delta^{13}C$ values at our Southern Hemisphere sites, because of the brevity of our record and the possible anomaly we may have observed in 1998. Conversely, seasonal cycle amplitudes in $\delta^{13}C$ much greater than 0.1 ‰ are an indication that processes other than destruction by OH are at work.

3.3.2. Northern Hemisphere Sites

Seasonal variations of $\delta^{13}C$ are more distinct in the NH than in the SH. Roughly 75% of methane emissions are from the Northern Hemisphere [*Fung et al.*, 1991]. Mean NH mole fractions average about 90 ppb higher than in the Southern Hemisphere, and in both 1998 and 1999 $\delta^{13}C$ values averaged about 0.3‰ lower in the NH than in the SH. The relative proximity of NH sampling sites to source regions also results in a greater degree of variability in the seasonal variations of both mole fractions and isotopic ratios than is observed in the SH.

Seasonal variations are most evident at BRW where the seasonal cycle amplitude has averaged 0.65‰, with the maximum in May and the minimum at the end of September. $\delta^{13}C$ values start to decrease in May and continue through the summer despite the fact that destruction of CH_4 by OH is largest during this time of year. This

probably occurs because emissions from isotopically light sources like wetlands are greatest during the summer, and bacterial emissions have 2-3 times the impact on $\delta^{13}C$ values than OH for the same change in mole fraction. Seasonal patterns at NWR and MLO are less distinct than at BRW, but as is the case in the SH exhibit deeper minima in 1998. The amplitudes are also substantially smaller than at BRW, which may be a result of BRW being closer to strong wetland emission regions.

3.4 Constraints on the global budget

The global atmospheric average $^{13}C/^{12}C$ (R_A) is related to the flux-weighted isotopic ratio of all sources (R_S) by

$$R_S = \frac{CR_A^{'} + R_A C^{'} + CR_A k_{12} \alpha}{C^{'} + Ck_{12}} \tag{3}$$

where C is the average atmospheric methane mole fraction, "prime" denotes time derivative, k_{12} is the inverse of the methane lifetime and α is k_{13}/k_{12}. The denominator is simply the total of all methane sources. Lassey *et al.* [1999] have formulated the same expression in the more usual δ notation:

$$\delta_S = \alpha\delta_A + \varepsilon - \frac{\varepsilon(1+\delta_A/1000)C^{'} + \delta_A^{'}C}{S} \tag{4}$$

where $\varepsilon = 1000(\alpha\text{-}1)$. These exact formulations differ from the common first order approximation

$$\delta_S = \delta_A + \varepsilon \tag{5}$$

Using average values for the parameters in (4) over the period of our measurements (Table 2), δ_S = -52.68 ‰. Using (5) the value would be –53.32 ‰. Global average δ_s is clearly sensitive to the approximations used its calculation. As would be

expected simply from (5), δ_s is most sensitive to δ_A and ε, although δ_A is better known than ε. ε requires knowledge of OH, soil, stratospheric and possibly Cl sink fractionation factors and their relative reaction rates, whereas δ_A can be directly measured. δ_s is not very sensitive to methane mole fraction and δ growth rates, but if we assume that they are zero, *i.e.* that the atmosphere is at steady-state with respect to both $^{13}CH_4$ and $^{12}CH_4$, the δ_s estimate may be in error by up to one per mil.

3.4.1 An Inverse Two-Box Model

We can use the annual average of observed values of $\delta^{13}C$ and CH_4 mole fraction in each hemisphere to constrain the global methane budget by simultaneously solving equations 6 and 7, and 8 and 9 for bacterial and biomass burning emission strengths in each hemisphere, if we calculate the strength of fossil fuel emissions on the basis of radiocarbon measurements [e.g., *Quay et al.*, 1999] and assume emissions of other small sources in each hemisphere. (6) – (9) are mass balances for $^{12}CH_4$ and $^{13}CH_4$ in each hemisphere.

$$C_N^{'} + k_{12}C_N + k_{ex}(C_N - C_S) - FFP_N = B_N + BMB_N \quad (6)$$

$$(C_N R_N)^{'} + \alpha k_{12} C_N R_N + k_{ex}(C_N R_N - C_S R_S) - R_3 FFP_N = R_1 B_N + R_2 BMB_N \quad (7)$$

$$C_S^{'} + k_{12}C_S - k_{ex}(C_N - C_S) - FFP_S = B_S + BMB_S \quad (8)$$

$$(C_S R_S)^{'} + \alpha k_{12} C_S R_S - k_{ex}(C_N R_N - C_S R_S) - R_3 FFP_S = R_1 B_S + R_2 BMB_S \quad (9)$$

Here, the subscripts N and S refer to each hemisphere, C to total methane mole fraction, *i.e.* $^{13}CH_4 + {}^{12}CH_4$, "prime" denotes the time derivative, and R is the isotopic ratio $^{13}C/(^{13}C + {}^{12}C)$. Note that this is not the standard way of defining R, so we must re-define $R_{PDB} = {}^{13}C/(^{13}C + {}^{12}C) = 0.01111$. k_{ex} is the inter-hemispheric exchange constant,

B is the total of all bacterial emissions, BMB the total of biomass burning emissions, and FFP the total of fossil fuel related emissions, plus other emissions, especially those from landfills. Fossil fuel and landfill sources were grouped together because of their very similar source distributions – both estimated to be more than 90% in the north. A composite isotopic ratio was created for this category by weighting their isotopic source signatures by emissions.

Table 2 lists values of parameters used in the equations. The left-hand-sides of (6) – (9) contain only known quantities and the four unknown fluxes are on the right-hand-side. When we solve our two systems of two linear equations using our best estimates for the terms on the left-hand-side, the global emission totals are: bacterial = 355 ± 48 Tg/yr, biomass burning = 56 ± 37 Tg/yr. The hemispheric totals are B_N=250 ± 33 Tg/yr, B_S=106 ± 21 Tg/yr, BMB_N=23 ± 30 Tg/yr and BMB_S=31 ± 10 Tg/yr. We calculate the ratio of the B, FFP, and BMB emissions as 65/25/10. This is similar to the ratios obtained by *Fung et al.* [1991] of 64/25/11, *Crutzen et al.* [1995] of 72/22/6, and by *Hein et al.* [1997] of 70/22/7.

We estimated errors using a Monte Carlo approach in which all parameters not determined from NOAA/CMDL measurements were assigned errors listed in Table 2. The dominant source of error appears to be the uncertainty in our assumption of fossil fuel emission rate, especially for Northern Hemisphere sources. Uncertainty in source δ values and rate coefficients for sinks are the next most important sources of error. The inter-hemispheric exchange constant, k_{ex}, does not influence global partitioning, but has a big impact on partitioning of a source between hemispheres. For example, although our

stronger BMB_S source contrasts with other estimates [e.g., *Fung et al.*, 1991], we can adjust the N/S partitioning by choosing a different value of k_{ex}.

The sensitivity of our model to changes in individual parameters is shown in Table 3. It is evident that improving the precision of our atmospheric measurements will not dramatically alter our ability to partition sources, at least when using annual hemispheric average $\delta^{13}C$ values. Changing the global average δ by 0.1‰ would only alter emissions partitioning by about 1.5 Tg/yr in our model. The hemispheric gradient in $\delta^{13}C$ can be an important constraint on hemispheric partitioning of sources provided that the inter-hemispheric exchange rate is well known, but the gradient doesn't strongly constrain global emission totals, only their north/south partitioning. The biggest improvements in emission partitioning will come from better constraining fossil fuel emissions as stated earlier by Quay *et al*. [1999], and by better understanding the isotopic ratio of source emissions and how and why they vary. Unless the value of ε_{OH} is in error by more than 2-3‰, the most important way we can improve the sink side of the equation is by better determining the lifetime of CH_4 in the atmosphere, including the magnitude of the soil sink. Our box model does not make use of seasonal and inter-annual variations in the data. As our monitoring effort continues and more data accumulates, seasonal variations and eventually long-term trends should provide additional constraints on the global budget.

3.4.2. Sensitivity to Tropospheric Chlorine

One way to improve our understanding of the lifetime of CH_4 is to establish the extent to which atomic Cl in the marine boundary layer (MBL) consumes CH_4. A variety of studies have suggested the possibility of CH_4 oxidation by Cl in the marine boundary

layer [*Gupta et al.*, 1996; *Vogt et al.*, 1996; *Wingenter et al.*, 1999; Allan et al.,. In Press,]. Wingenter *et al.* [1999] estimated that 2% of CH_4 in the MBL is consumed by Cl. Because of the unusually large isotopic fractionation that results when CH_4 reacts with Cl [*Saueressig et al.*, 1995], atmospheric $\delta^{13}C$ is a good tracer for the presence of Cl radical. In a model experiment, we introduced a Cl sink for atmospheric CH_4 that was scaled according to ocean surface area in each hemisphere. Using the parameters in Table 2, our results indicate that a small tropospheric Cl sink cannot be ruled out (Figure 9). If the Cl sink in the troposphere were greater than 6 ± 4% of the total sink, then the biomass burning source would be less than 20 Tg/yr, which is unlikely from an inventory point of view. We generate the error estimate by incorporating the 50% error in our fossil fuel emission estimate into our calculation.

3.5 Comparison of NOAA/INSTAAR Data with Other Records

Maximal use of our measurements will come when they can be confidently integrated with existing records [*Quay et al.*, 1991, 1999; *Lowe et al.*, 1994; *Francey et al.*, 1999; *Tyler et al.*, 1999]. At present, no common standard scale for $\delta^{13}CH_4$ in air exists, making comparisons between different laboratories difficult. Nonetheless, we present a comparison of our data from BRW, MLO, SMO and CGO with those of Quay *et al.* [1999] from 1988 – 1996 in Figure 10. A line is fit through the Quay data to represent the small positive trend. Extrapolating the trend in the $\delta^{13}C$ data to bridge the 1.5 year gap between our data and the Quay data suggests that our data are heavier than the Quay data by about 0.1‰. The atmospheric $\delta^{13}C$ trend may have changed markedly in the 1.5 year period when $\delta^{13}C$ values were not being measured at MLO, SMO, and

BRW, but without a direct inter-comparison of standards and air samples, the magnitude of the offset between the two labs will be difficult to determine.

At CGO, our 1998 annual mean value of –46.96‰ is also about 0.1‰ heavier than the fitted trend curve of the CGO archived air samples [*Francey et al.*, 1999]. Figure 11 shows our 1998 CGO data alongside the 10 year record from Baring Head, New Zealand (41 S), and shorter records from CGO. After extrapolating the positive $\delta^{13}C$ trend between 1992 and 1998, our CGO data appear to be about 0.1‰ heavier. Our CGO data also appear to be about 0.1 ‰ heavier than data from Baring Head, New Zealand during 1998 and 1999 [D. Lowe, personal communication]. Samples collected at NWR by our lab and the Tyler lab during 1998 compare well [S. Tyler, personal communication.]. Samples were collected on different days, at different times, and at a different location on Niwot Ridge precluding a direct comparison, but there is no obvious offset in the data. This is expected because both labs use a scale prepared by the Tyler lab. The apparent agreement between our lab and the Tyler lab exist despite the good agreement on samples measured in common between the Tyler lab and the NIWA lab [*Tyler et al.*, 1999]. These offsets emphasize the need to inter-compare measurements between different laboratories through joint measurements of whole air in both reference tanks and sample flasks.

4. Conclusion

We have presented a spatially and temporally dense data set of atmospheric $\delta^{13}C$ values available. This was enabled by the development of an automated, high-precision gas chromatography – isotope ratio mass spectrometry technique that was coupled with the NOAA/CMDL global air sampling network. The global mean $\delta^{13}C$ value during

1998-1999 was -47.10‰, and the Northern and Southern Hemisphere means were –47.28‰ and –46.93‰, respectively. Southern Hemisphere $\delta^{13}C$ values show very little meridional variability, while in the Northern Hemisphere, there is a difference of about 0.4‰ between MLO and BRW. The annual average difference measured between SPO and BRW was 0.6‰.

Northern Hemisphere seasonal variations are more complex than those in the Southern Hemisphere, reflecting the proximity to seasonally varying source emissions and more complex atmospheric circulation. Summertime $\delta^{13}C$ variations at all of the NH sites, but especially BRW and NWR, appear to be dominated by changes in isotopically light emissions, possibly from wetlands. In the Southern Hemisphere, seasonal variations have been less consistent. During 1998 $\delta^{13}C$ variations are too large to be explained solely by changes in OH and may be the result of enhanced tropical wetlands emissions. In other years our level of measurement precision may be preventing us from observing seasonal cycles in the Southern Hemisphere.

Since January 1998 we have analyzed more than 600 pairs of flasks with analytical precision sufficient to determine the meridional gradient and observe seasonal variations in the Northern Hemisphere. One of the principal challenges in the near future will be to establish the magnitude of any offsets of our measurements relative to other laboratories making similar measurements. All of our current measurements are based on reference air tanks calibrated by the Tyler lab at the University of California, Irvine. However, there are some preliminary indications that our values may be heavier than those of the Quay lab [e.g., *Quay et al.*, 1991; 1999] and the NIWA (New Zealand) lab

[*Lowe et al.*, 1994; *Francey et al.*, 1999] by 0.1‰, but without direct comparisons, this is difficult to establish.

We have used a two-box model to show how our $\delta^{13}C$ measurements coupled with methane mole fraction measurements made on the same samples can provide some constraints on the global methane budget. Making use of the more detailed spatial and seasonal variations present in our data should provide better constraints on the global methane budget. Prediction of future amounts of methane in the atmosphere is predicated on a detailed understanding of the global source and sink processes and how they change over time. Atmospheric $\delta^{13}C$ measurements can help to achieve this goal, if we can (1) improve our understanding of the isotopic ratio of emissions from sources (2) better define CH_4 lifetime with respect to different sinks and their fractionation factors and (3) couple $\delta^{13}C$ measurements with radiocarbon and δD measurements.

References:

Allan, W., M.R. Manning, K.R. Lassey, D.C. Lowe, and A.J. Gomez, Modeling the variation of $\delta^{13}C$ in atmospheric methane: Phase ellipses and kinetic isotope effect, *Global Biogeochem. Cycles*, In Press.

Blunier, T., J.A. Chappellaz, J. Schwander, J.M. Barnola, T. Desperts, B. Stauffer, and D. Raynaud, Atmospheric Methane, Record From a Greenland Ice Core Over the Last 1000 Year, *Geophys. Res. Lett.*, *20*(20), 2219-2222, 1993.

Brown, M., Deduction of Emissions of Source Gases Using an Objective Inversion Algorithm and a Chemical-Transport Model, *J. Geophys. Res.*, *98*(D7), 12639-12660, 1993.

Burgoyne, T.W., and J.M. Hayes, Quantitative production of H-2 by pyrolysis of gas chromatographic effluents, *Anal. Chem.*, *70*(24), 5136-5141, 1998.

Cantrell, C.A., R.E. Shetter, A.H. McDaniel, J.G. Calvert, J.A. Davidson, D.C. Lowe, S.C. Tyler, R.J. Cicerone, and J.P. Greenberg, Carbon Kinetic Isotope Effect in the Oxidation of Methane By the Hydroxyl Radical, *J. Geophys. Res.*, *95*(D13), 22455-22462, 1990.

Cicerone, R.J., and R.S. Oremland, Biogeochemical aspects of atmospheric methane, *Global Biogeochem. Cycles*, *2*, 299-327, 1988.

Conny, J.M., and L.A. Currie, The isotopic characterization of methane, non-methane hydrocarbons and formaldehyde in the troposphere, *Atmospheric Environment*, *30*(4), 621-638, 1996.

Conway, T.J., P.P. Tans, L.S. Waterman, K.W. Thoning, D.R. Kitzis, K.A. Massarie, and N. Zhang, Evidence for interannual variability of the carbon cycle for the National

Oceanic and Atmospheric Administration/Climate Monitoring Diagnostics Laboratory Global Air Sampling Network, *J. Geophys. Res.*, *99*(D11), 22,831-22,855, 1994.

Coplen, T.B., Discontinuance of SMOW and PDB, *Nature*, *375*(6529), 285-285, 1995.

Dlugokencky, E.J., K.A. Masarie, P.M. Lang, and P.P. Tans, Continuing decline in the growth rate of the atmospheric methane burden, *Nature*, *393*(6684), 447-450, 1998.

Dlugokencky, E.J., L.P. Steele, P.M. Lang, and K.A. Masarie, The Growth-Rate and Distribution of Atmospheric Methane, *J. Geophys. Res.*, *99*(D8), 17021-17043, 1994.

Dlugokencky, E.J., B.P. Walter, and E.S. Kaischke, Measurements of an anomalous global methane increase during 1998, *Geophys. Res. Lett.*, *28*(3), 499-503, 2001.

Etheridge, D.M., G.I. Pearman, and P.J. Fraser, Changes in Tropospheric Methane Between 1841 and 1978 From a High Accumulation-Rate Antarctic Ice Core, *Tellus, Ser. B*, *44*(4), 282-294, 1992.

Etheridge, D.M., L.P. Steele, R.J. Francey, and R.L. Langenfelds, Atmospheric methane between 1000 AD and present: Evidence of anthropogenic emissions and climatic variability, *J. Geophys. Res.*, *103*(D13), 15979-15993, 1998.

Francey, R.J., M.M. Manning, C. Allison, E., S.A. Coram, D.M. Etheridge, R.L. Langenfelds, D.C. Lowe, and L.P. Steele, A history of $\delta^{13}C$ in atmospheric CH_4 from the Cape Grim Air Archive and Antarctic firn air., *J. Geophys. Res.*, *In press*, 1999.

Fung, I., J. John, J. Lerner, E. Matthews, M. Prather, L.P. Steele, and P.J. Fraser, 3-Dimensional Model Synthesis of the Global Methane Cycle, *J. Geophys. Res.*, *96*(D7), 13033-13065, 1991.

Gupta, M., S. Tyler, and R. Cicerone, Modeling atmospheric $\delta^{13}CH_4$ and the causes of recent changes in atmospheric CH_4 amounts, *J. Geophys. Res.*, *101*(D17), 22,923-22,932, 1996.

Hein, R., P.J. Crutzen, and M. Heimann, An inverse modeling approach to investigate the global atmospheric methane cycle, *Global Biogeochem. Cycles*, *11*(1), 43-76, 1997.

Hilkert, A.W., C.B. Douthitt , H.J. Schluter, and W.A. Brand, Isotope ratio monitoring gas chromatography mass spectrometry of D/H by high temperature conversion isotope ratio mass spectrometry, *Rapid Comm. Mass. Spec.*, *13*, 1226-1230, 1999.

Houweling, S., T. Kaminski, F. Dentener, J. Lelieveld, and M. Heimann, Inverse modeling of methane sources and sinks using the adjoint of a global transport model, *J. Geophys. Res.*, *104*(D21), 26,173-26,160, 1999.

Jones, R.L., and J.A. Pyle, Observations of CH4 and N2 O by the Nimbus-7 SAMS: a comparison with in situ data and two-dimensional numerical model calculations, *J. Geophys. Res.*, *89*(D4), 5263-5279, 1984.

King, S.L., P.D. Quay, and J.M. Lansdown, The C-13/C-12 Kinetic Isotope Effect For Soil Oxidation of Methane At Ambient Atmospheric Concentrations, *J. Geophys. Res.*, *94*(D15), 18273-18277, 1989.

Lang, P., L.P. Steele, and R.C. Martin, Atmospheric methane data for the period 1986-1988 from the NOAA/CMDL global cooperative flask sampling network, pp. 108, NOAA Climate Monitoring and Diagnostics Laboratory, Boulder, 1990.

Lashof, D.A., and D.R. Ahuja, Relative Contributions of Greenhouse Gas Emissions to Global Warming, *Nature*, *344*(6266), 529-531, 1990.

Lassey, K.R., D.C. Lowe, and M.R. Manning, The trend in atmospheric methane $\delta^{13}C$ and implications for isotopic constraints on the global methane budget, *Global Biogeochem. Cycles*, *In press*, 1999.

Law, R., I. Simmonds, and W.F. Budd, Application of an Atmospheric Tracer Model to High Southern Latitudes, *Tellus, Ser. B.*, *44*(4), 358-370, 1992.

Lowe, D.C., W. Allan, M.R. Manning, T. Bromley, G. Brailsford, D. Ferretti, A. Gomez, R. Knobben, R. Martin, Z. Mei, R. Moss, K. Koshy, and M. Maata, Shipboard determinations of the distribution of d13C in atmospheric methane in the Pacific, *J. Geophys. Res.*, *104*(D21), 26,125-26,135, 1999.

Lowe, D.C., C.A.M. Brenninkmeijer, G.W. Brailsford, K.R. Lassey, A.J. Gomez, and E.G. Nisbet, Concentration and C-13 Records of Atmospheric Methane in New-Zealand and Antarctica - Evidence For Changes in Methane Sources, *J. Geophys. Res.*, *99*(D8), 16913-16925, 1994.

Lowe, D.C., C.A.M. Brenninkmeijer, S.C. Tyler, and E.J. Dlugokencky, Determination of the Isotopic Composition of Atmospheric Methane and Its Application in the Antarctic, *J. Geophys. Res.*, *96*(D8), 15455-15467, 1991.

Lowe, D.C., M.R. Manning, G.W. Brailsford, and A.M. Bromley, The 1991-1992 atmospheric methane anomaly: Southern Hemisphere C-13 decrease and growth rate fluctuations, *Geophys. Res. Lett.*, *24*(8), 857-860, 1997.

Merritt, D.A., J.M. Hayes, and D.J. Des Marais, Carbon isotopic analysis of atmospheric methane by isotope-ratio-monitoring gas chromatography-mass spectrometry, *J. Geophys. Res.*, *100*(D1), 1317-1326, 1995.

Myhre, G., E.J. Highwood, K.P. Shine, and F. Stordal, New estimates of radiative forcing due to well mixed greenhouse gases, *Geophys. Res. Lett.*, *25*, 2715-2718, 1998.

Quay, P., J. Stutsman, D. Wilbur, A. Snover, E. Dlugokencky, and T. Brown, The isotopic composition of atmospheric methane, *Global Biogeochem. Cycles*, *13*(2), 445-461, 1999.

Quay, P.D., S.L. King, J. Stutsman, D.O. Wilbur, L.P. Steele, I. Fung, R.H. Gammon, T.A. Brown, G.W. Farwell, P.M. Grootes, and F.H. Schmidt, Carbon isotopic composition of atmospheric CH_4: Fossil and biomass burning source strengths, *Global Biogeochem. Cycles*, *5*, 25-47, 1991.

Sansone, F., J., B. Popp, N., and T. Rust, M., Stable Carbon Isotopic Analysis of Low-Level Methane in Water and Gas, *Anal. Chem.*, *69*, 40-44, 1997.

Saueressig, G., P. Bergamaschi, J.N. Crowley, H. Fischer, and G.W. Harris, Carbon Kinetic Isotope Effect in the Reaction of Ch4 With Cl Atoms, *Geophys. Res. Lett.*, *22*(10), 1225-1228, 1995.

Steele, L.P., E.J. Dlugokencky, P.M. Lang, P.P. Tans, R.C. Martin, and K.A. Masarie, Slowing Down of the Global Accumulation of Atmospheric Methane During the 1980s, *Nature*, *358*(6384), 313-316, 1992.

Steele, L.P., P.J. Fraser, R.A. Rasmussen, M.A.K. Khalil, T.J. Conway, A.J. Crawford, R.H. Gammon, K.A. Masarie, and K.W. Thoning, The Global Distribution of Methane in the Troposphere, *J. Atmos. Chem.*, *5*(2), 125-171, 1987.

Stevens, C.M., Carbon-13 isotopic abundance and concentration of atmospheric methane for background air in the southern and northern hemispheres from 1978 to 1989, , *Publication 4388*(Environmental Science Division, U.S. Dept. of Energy), 1995.

Stevens, C.M., and F.E. Rust, The Carbon Isotopic Composition of Atmospheric Methane, *J. Geophys. Res.*, *87*(c7), 4879-4882, 1982.

Thompson, A.M., The oxidizing capacity of the earth's atmosphere: probable past and future changes, *Science, 256*, 1157-1165, 1992.

Thoning, K.W., P.P. Tans, and W.D. Komhyr, Atmospheric carbon dioxide at Mauna Loa Observatory 2. Analysis of the NOAA GMCC data, 1974-1985, *J. Geophys. Res.*, *94*, 8549-8565, 1989.

Tyler, S.C., Stable Carbon Isotope Ratios in Atmospheric Methane and Some of its Sources, *J. Geophys. Res.*, *91*(D12), 13,232-12,238, 1986.

Tyler, S.C., H.O. Ajie, M.L. Gupta, R.J. Cicerone, D.R. Blake, and E.J. Dlugokencky, Carbon isotopic composition of atmospheric methane: A comparison of surface level and upper tropospheric air, *J. Geophys. Res.*, *In Press*, 1999.

Vogt, R., P.J. Crutzen, and R. Sander, A mechanism for halogen release from sea-salt aerosol in the remote marine boundary layer, *Nature*, *383*, 327-330, 1996.

Wingenter, O.W., D.R. Blake, N.J. Blake, B.C. Sive, F.S. Rowland, E. Atlas, and F. Flocke, Tropospheric hydroxyl radical and atomic chlorine concentrations, and

mixing timescales determined from hydrocarbon and halocarbon measurements made over the Southern Ocean, *J. Geophys. Res.*, *104*(D17), 21,819-21,828, 1999.

Zeng, Y., H. Mukai, H. Bandow, and Y. Nojiri, Application of gas chromotography-combustion-isotope ratio mass spectrometry to carbon isotopic analysis of methane and carbon monoxide in environmental samples, *Analytical Chimica Acta, 289*, 195-204, 1994.

Figure Captions

1. Plumbing diagram for methane separation and combustion apparatus.

2. Methane pre-concentration device. CH_4 is trapped at –120ºC, and bulk "air" is vented, after which CH_4 is released by heating to 0ºC. Cooling by liquid nitrogen and heating by NiCr wire are controlled by a temperature controller.

3. Typical peaks of m/z = 44 (thick line) and m/z = 45 (thin line, x 100) from a reference air or sample air run showing CH_4-derrived CO_2 chromatographic peak and the reference CO_2 peak admitted from the bellows of the mass spectrometer. Time is relative to the injection of the pre-concentrated sample onto the cryo-focus region of the analytical column.

4. Histogram showing the distribution of differences in δ values between pairs of flasks collected at the same time. (1^{st} flask – 2^{nd} flask). The super-imposed gaussian has a width of sigma = 0.08‰.

5. Standard deviation of reference air aliquots during batch analyses over time. Squares represent rejected runs and circles are retained. Solid line is the long-term mean of retained runs, 0.08 ‰.

6. Pair averaged data from all sites in this study. Solid line is the "smooth curve" fit (see text for details) to the retained pair averages (squares). Triangle are those data determined not to be representative of background atmospheric conditions. Rejected data are not plotted. Error bars are 0.08‰x$\sqrt{2}$, the mean standard deviation of a pair of samples.

7. Annual mean latitudinal gradient for $\delta^{13}C$ and methane mole fraction. Lines are cubic fits to the data.

8. Monthly mean $\delta^{13}C$ and mole fractions derived from smooth curve fit to the data for all sites used in this study. Error bars are one sigma standard deviation of smooth curve data used to calculate the means.

9. Calculated bacterial (solid line) and biomass burning (long dashes) emissions in the presence of a tropospheric Cl sink. We assume that fossil fuel emissions (short dashes) are constant.

10. Comparison of long-term measurements from U. Washington (Quay *et al.* 1999, squares) and this study (pluses) at four common sampling sites. Lines are least squares fits to Quay *et al.* data, used to extrapolate the trend to the period of this study.

11. Comparison of long-term measurements at Baring Head, New Zealand (41ºS) (Lowe *et al.*, 1994, squares) with data from this study at Cape Grim, Tasmania (41ºS). Line is a least squares fit to Baring Head data after 1992.

Table 1. NOAA/CMDL Air Sampling Sites Used in this Study

Site Code	Site	Country	Latitude	Longitude	Elevation (m)
BRW	Barrow, AK	USA	71º19' N	156º36' W	11
CGO	Cape Grim, Tasmania	Australia	40º41' S	144º41' E	94
MLO	Mauna Loa, HI	USA	19º32' N	155º35' W	3397
NWR	Niwot Ridge, CO	USA	40º03' N	105º38' W	3749
SMO	American Samoa	USA	14º15' S	170º34' W	42
SPO	South Pole	South Pole	89º59'	24º48' W	2810

Table 2. Input parameters for two-box model.

	C'^{a}	C^{a}	δ^{b}	δ^{a}	k_{ex}	$k_{12}{}^{c}$	α^{d}	FFP[e]	$\delta_B{}^{f}$	$\delta_{BMB}{}^{f}$	$\delta_{FFP}{}^{f}$
units	(ppb/yr)	(ppb)	(‰/yr)	(‰)	(1/yr)	(1/yr)		(Tg/yr)	(‰)	(‰)	(‰)
N	5.5	1791	0.02 ± 0.02	-47.2	1.0 ± 0.1	0.1071 ± 0.01	0.9936 ± 0.0008	124 ± 47	-61 ± 2	-24 ± 2	-43 ± 2
S	10.0	1705	0.02 ± 0.02	-46.9	1.0 ± 0.1	0.1057 ± 0.01	0.9938 ± 0.0008	11 ± 4	-61 ± 2	-24 ± 2	-43 ± 2

a. Average of measured values from NOAA/CMDL global network during 1998 - 1999.

b. From Quay *et al.* [1999]

c. Calculated as $k_{12}=k_{OH} + k_{SOIL}+ k_{STRAT}$. k_{OH} is 1/10.5 and is taken from Montzka *et al.* [2000]; k_{SOIL} was 1/484.2 and was calculated as a first-order loss assuming a 30 Tg/yr soil sink and a global CH_4 burden of 1750 ppb. We assume that 2/3 of the soil sink is in the Northern Hemisphere. k_{STRAT} is 1/110 and is taken from Scientific Assessment of Ozone Depletion: 1998.

d. Calculated as $\alpha=(\alpha_{OH}k_{OH} + \alpha_{SOI}k_{SOIL}+ \alpha_{STRAT}k_{STRAT})/k_{12}$. α_{OH} is 0.9946 and is taken from Cantrell *et al.* [1990]; α_{SOIL} is 0.979 and is taken from King *et al.* [1999]; α_{STRAT} is 0.988 and was calculated by weighting α_{OH} and α_{Cl} by the strengths of Cl and OH sinks in the stratosphere according to Hein *et al.* [1997]. Errors were determined only by propogating errors in k_{12} and assigning an error to α_{OH} of 0.0009, the error estimate of Cantrell *et al.* [1990].

e. FFP is the sum of the Fung *et al.* [1991] categories: gas venting, gas leaks, coal mining, and landfills. The total of the fossil fuel categories was 100 Tg/yr and was calculated from Quay *et al.* [1999] $^{14}CH_4$ data. Landfill emissions are taken as 35 Tg/yr, which is the average of the Hein *et al.* [1997] and Fung *et al.* [1991] estimates. The north/south division (92%/8%) is based on Table 4 of Fung *et al.* [1991]. The error estimates are derived from the range in landfill emission estimates (20 Tg/yr) and the range for fossil fuel emissions of 50% given in Quay *et al.* [1999].

f. B (Bacterial emissions) are defined as the sum of the Fung *et al.* categories: bogs, swamps, tundra, rice, animals, termites and clathrates; BMB is biomass burning; FFP defined as above. δ values were calculated using source signatures from Table 1 of Quay *et al.* with weightings from the global totals of the Fung *et al.* categories listed above. We assume that source signatures are the same for each hemisphere.

Table 3. Sensitivity of source partitioning to parameter changes in the inverse box-model.

Parameter	Units	Emission Source	Globally	NH	SH
δ_{SOURCE}	Tg ‰$^{-1}$	B	-14.2	-11.1	-3.1
δ_N-δ_S	Tg ‰$^{-1}$	B	0	69	-69
C_N-C_S	Tg ppb^{-1}	B	0	0.91	-0.91
%Cl added	Tg %$^{-1}$	B	11.2	3.9	7.3
		BMB[a]	-6.3	-2.2	-4.1
δ_B	Tg ‰$^{-1}$	B	9.7	7.3	2.4
δ_{BMB}	Tg ‰$^{-1}$	B	1.5	0.95	0.55
δ_{FFP}	Tg ‰$^{-1}$	B	6.7	6.3	0.4
FFP	Tg Tg^{-1}	B	-0.51	-0.47	-0.04
dδ/dt	Tg ‰$^{-1}$yr^{-1}	B	131	-67	-64
dC/dt	Tg ppb^{-1}yr^{-1}	B	1.7	0.9	0.8

a. For all other source sensitivities, BMB (biomass burning) is simply of the opposite sign as B (bacterial), such that total global emissions remain constant. Adding a Cl sink increases the total emissions in the model, which requires that BMB and B sensitivities not be of equal magnitude.

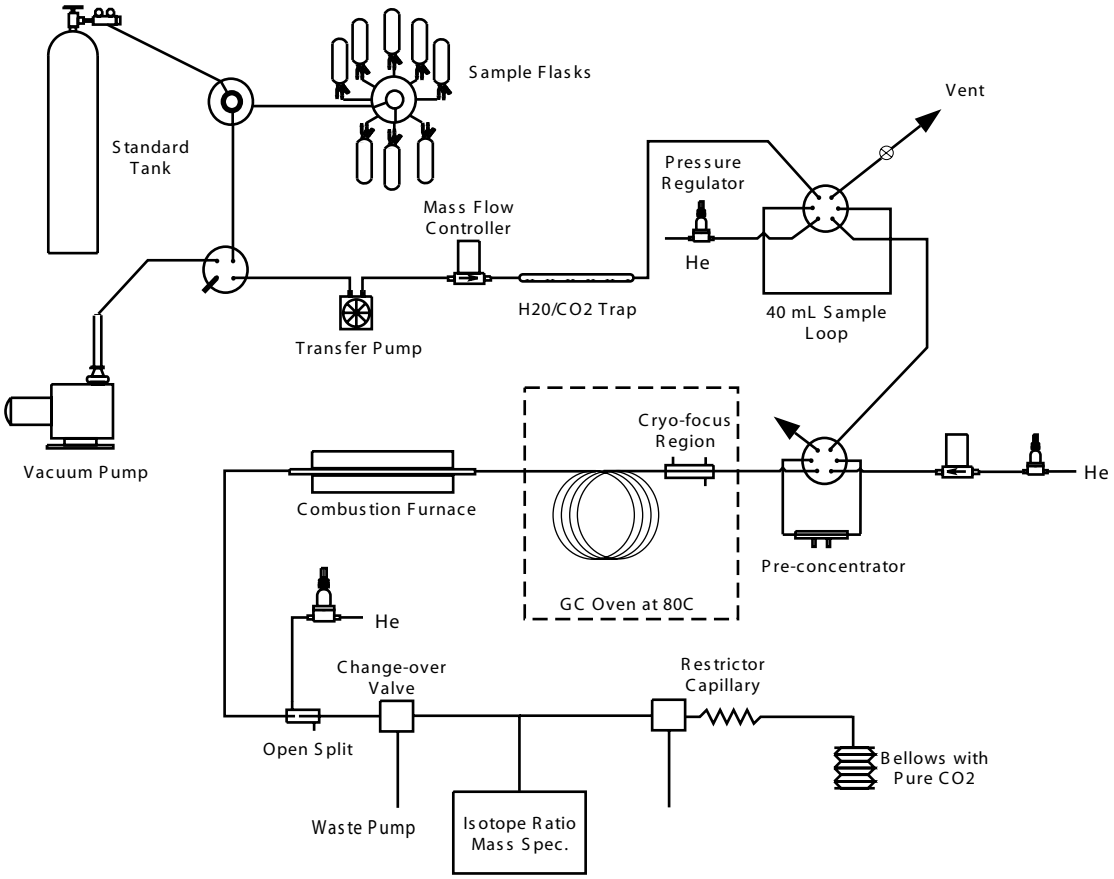
Sample Flasks
Vent
Standard Tank
Pressure Regulator
Mass Flow Controller
He
H20/CO2 Trap
40 mL Sample Loop
Transfer Pump
Vacuum Pump
Cryo-focus Region
He
Combustion Furnace
Pre-concentrator
GC Oven at 80C
He
Change-over Valve
Restrictor Capillary
Open Split
Bellows with Pure CO2
Waste Pump
Isotope Ratio Mass Spec.

Figure 1

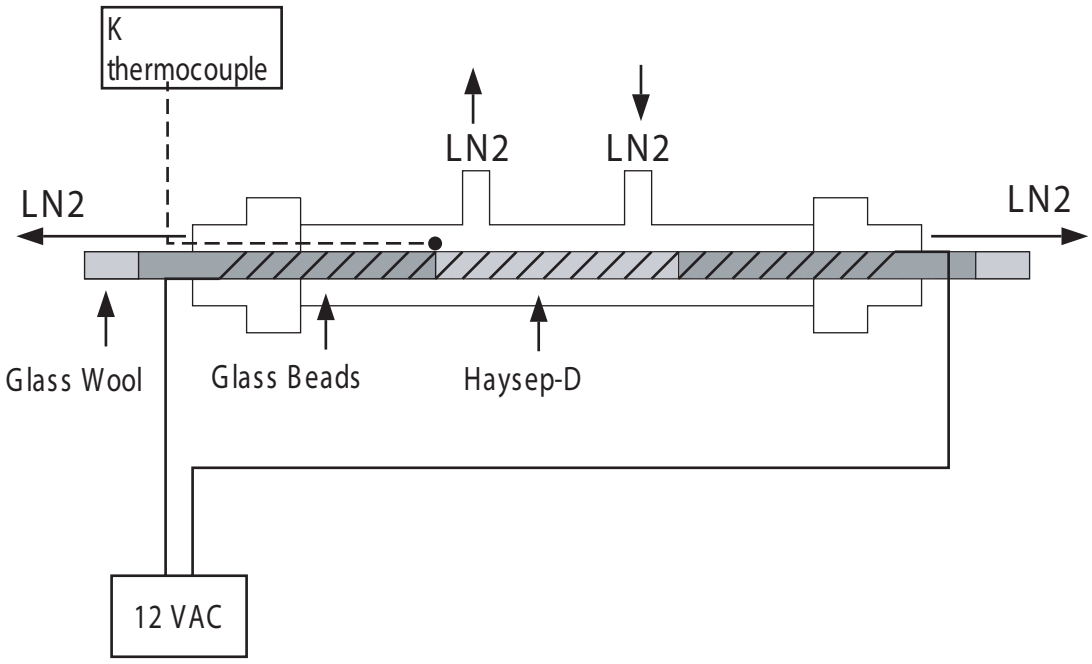
K
thermocouple
LN2
LN2
LN2
LN2
Glass Wool
Glass Beads
Haysep-D
12 VAC

Figure 2

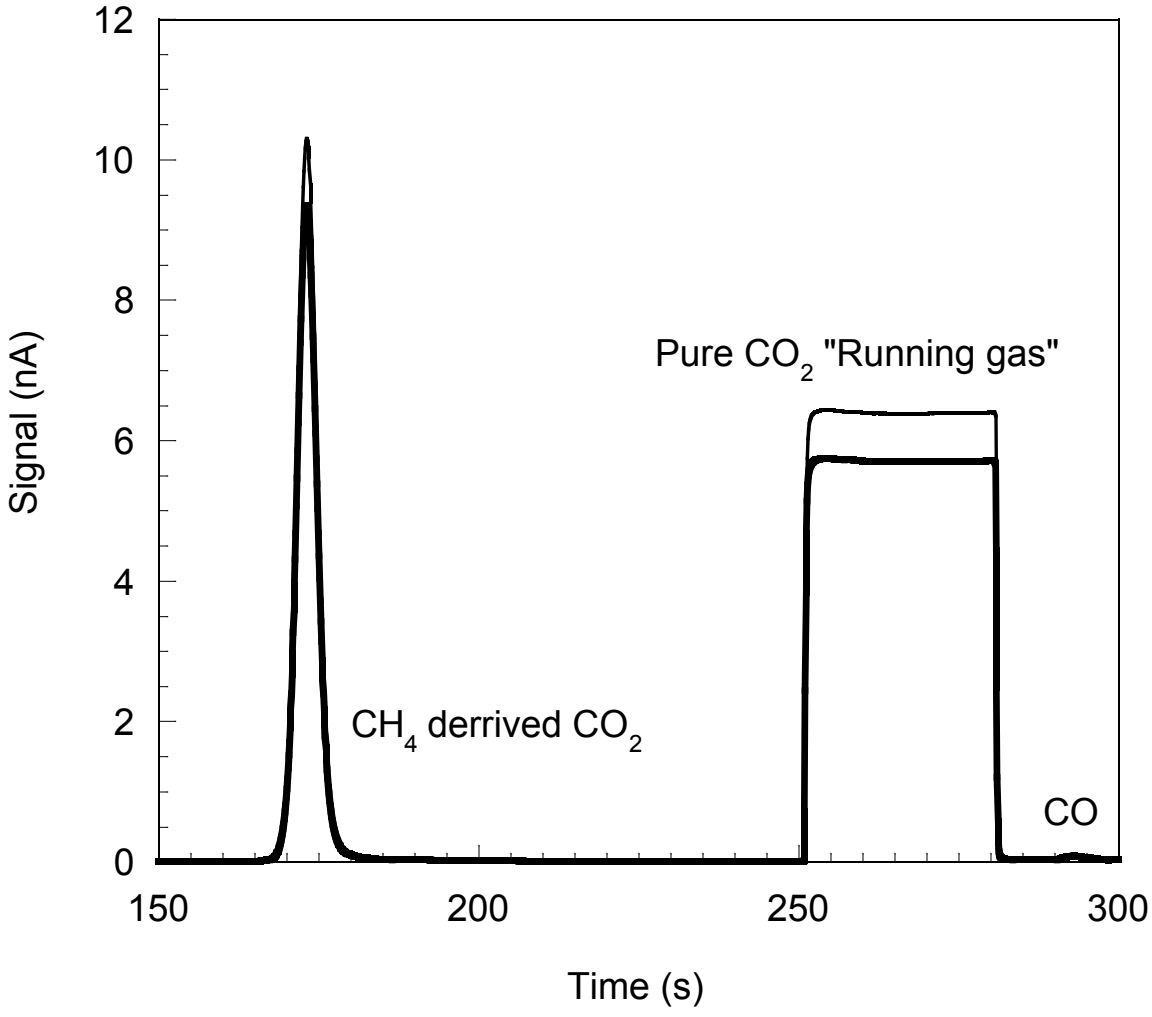
12
10
8
6
4
2
0
Signal (nA)
Pure CO_2 "Running gas"
CH_4 derrived CO_2
CO
150
200
250
300
Time (s)

Figure 3

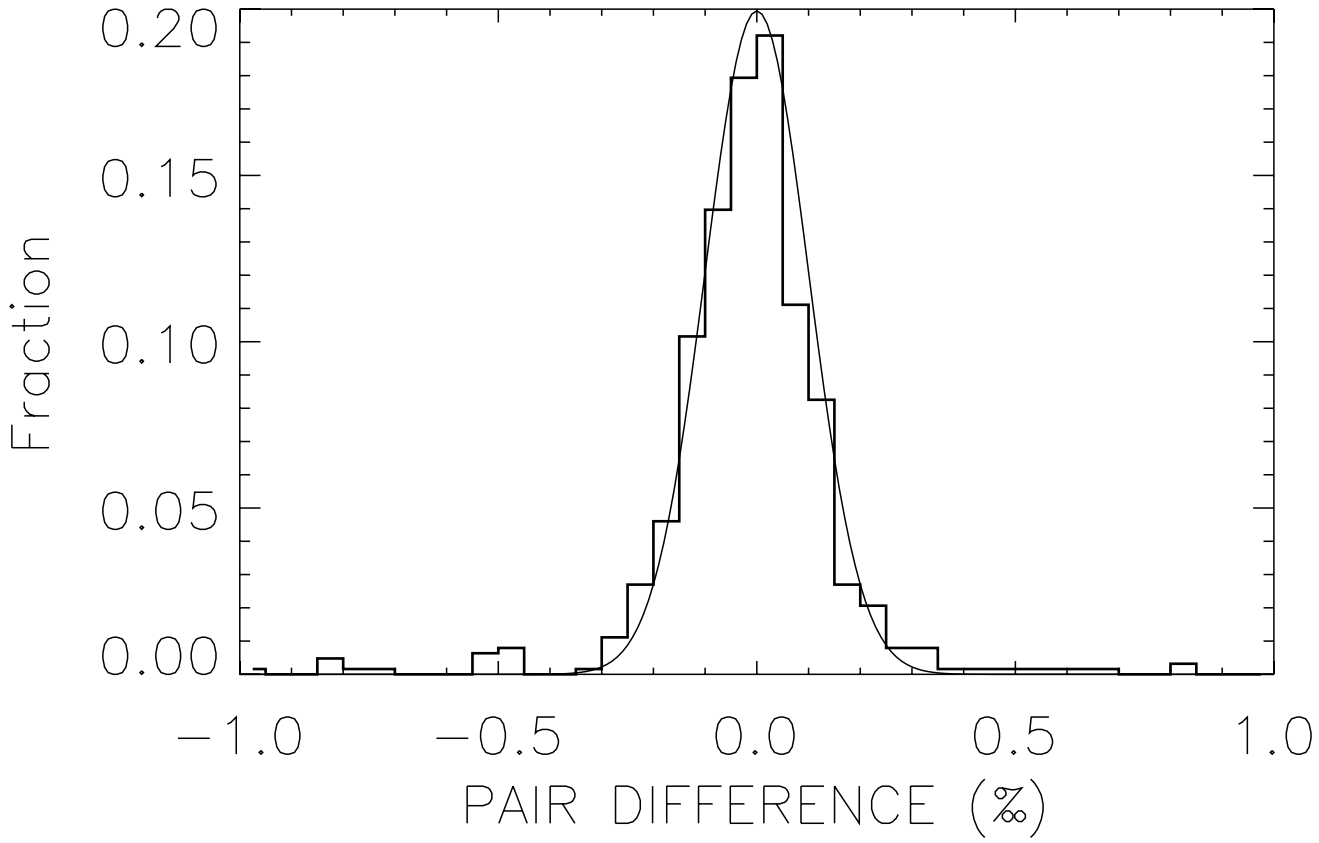

Figure 4

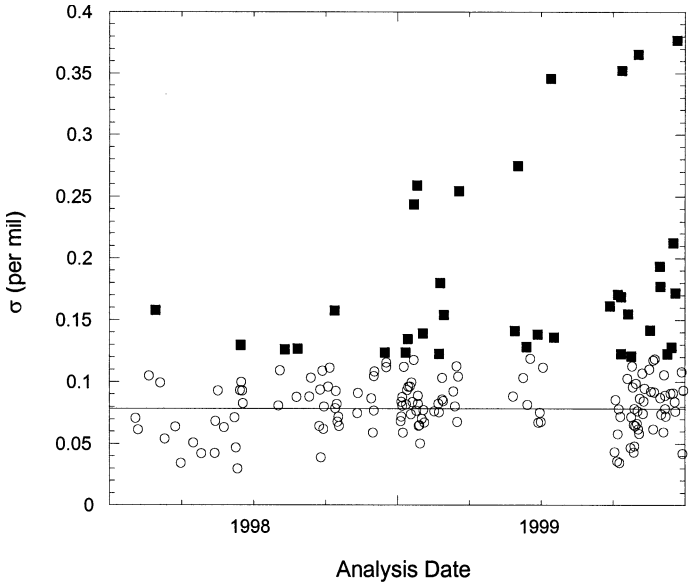

Figure 5

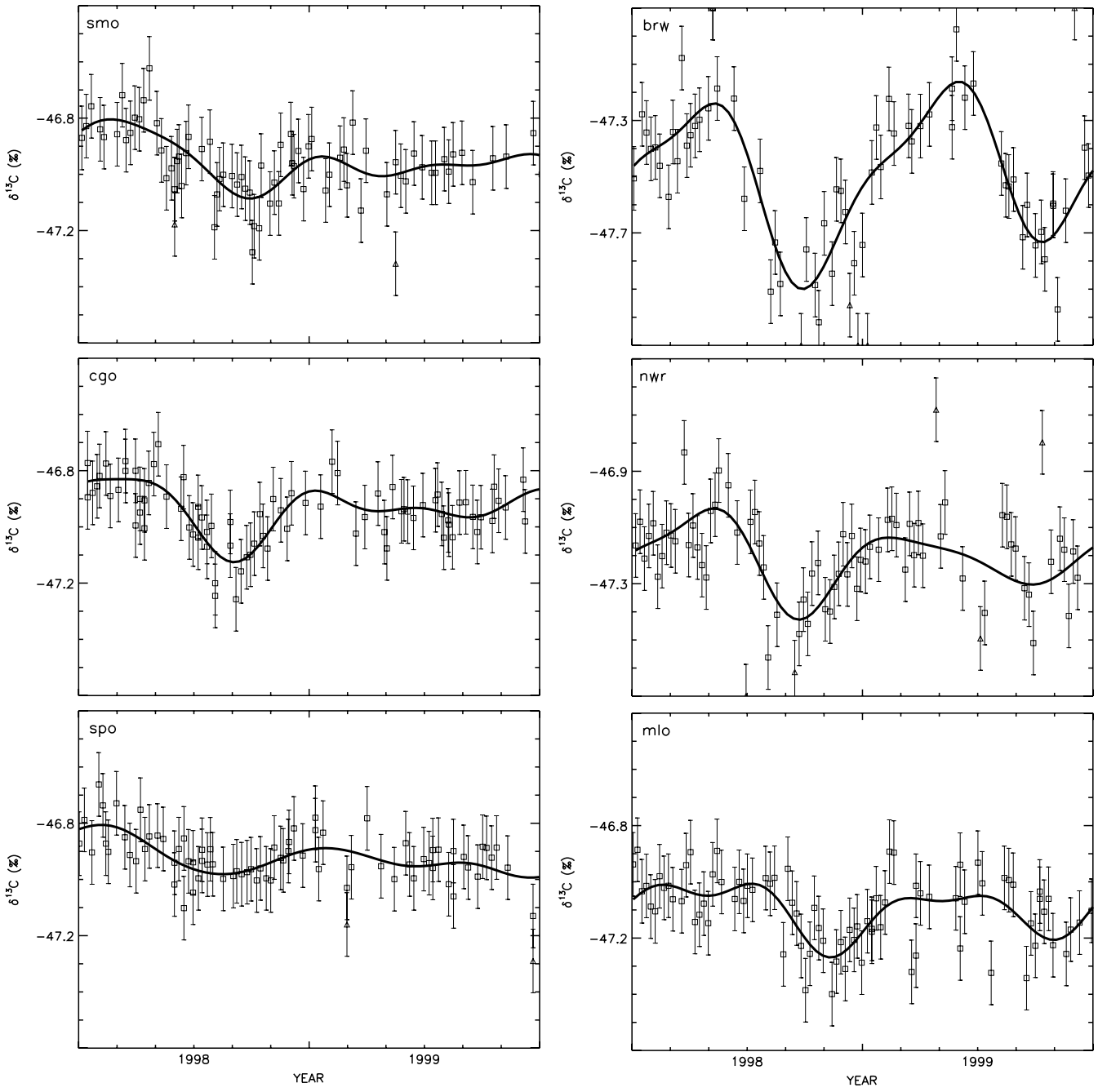

Figure 6

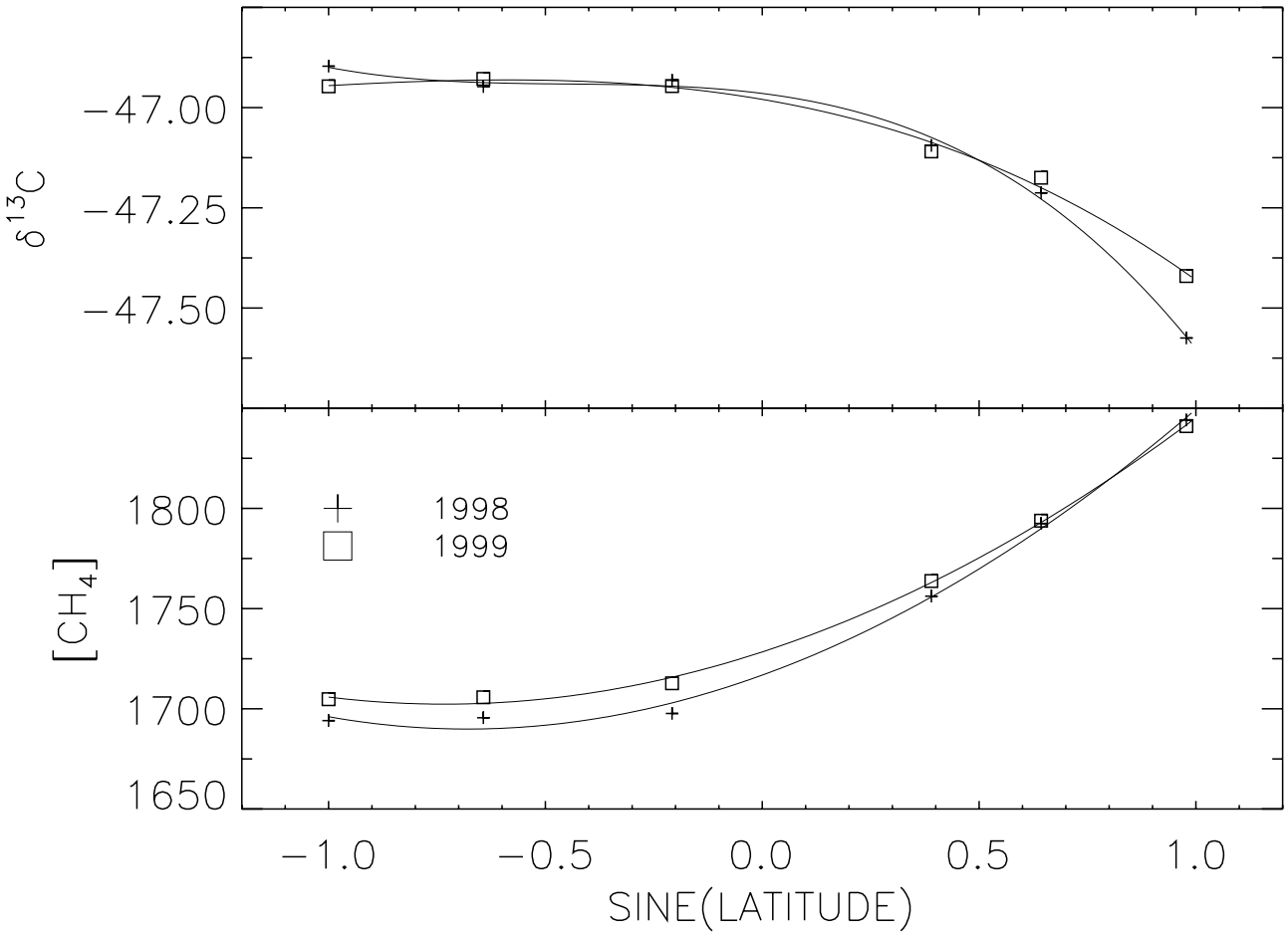
−47.00
−47.25
−47.50
δ13C
1800
1750
1700
1650
[CH4]
1998
1999
−1.0
−0.5
0.0
0.5
1.0
SINE(LATITUDE)

Figure 7

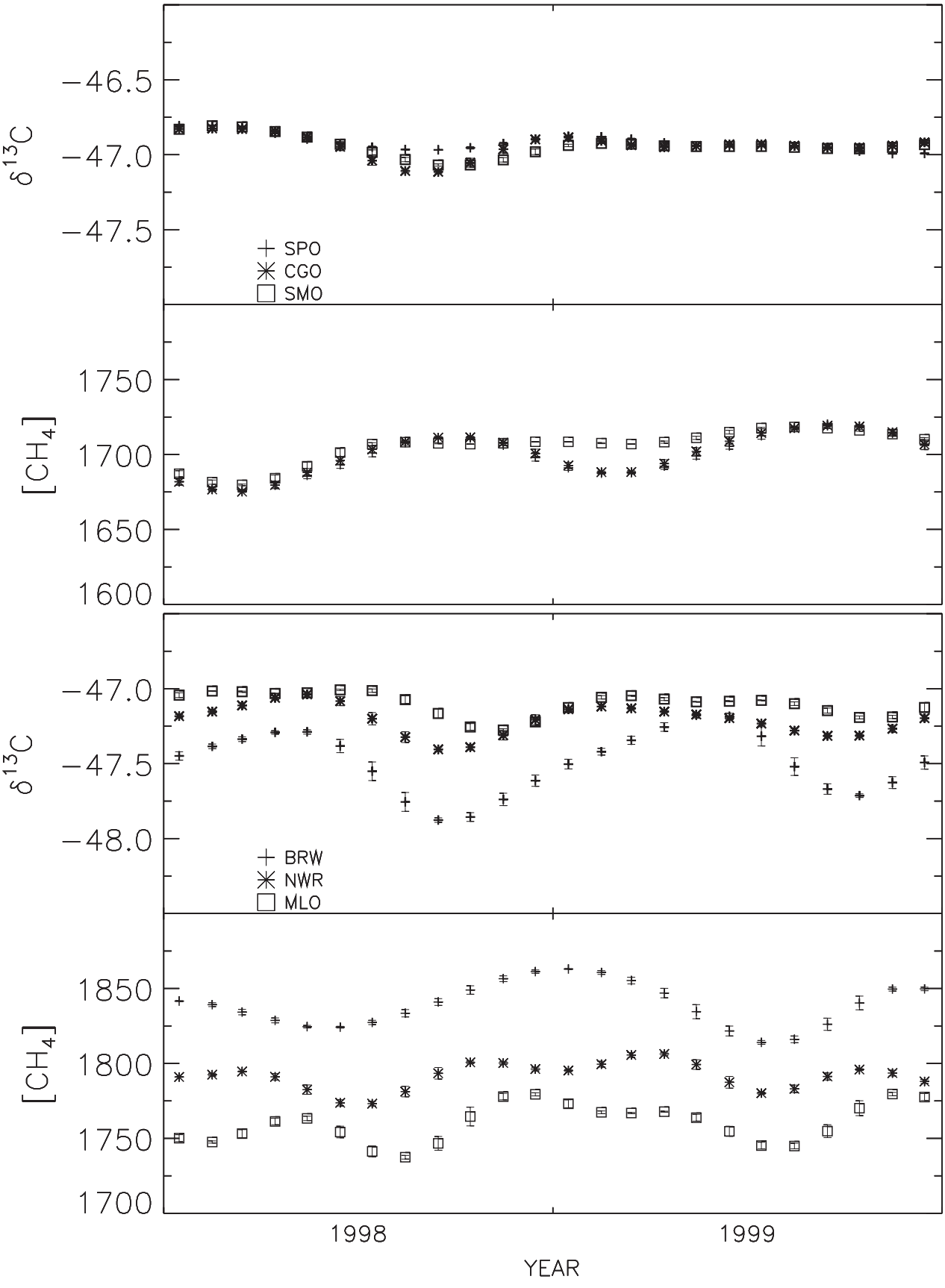
δ13C
−46.5
−47.0
−47.5
SPO
CGO
SMO
[CH4]
1750
1700
1650
1600
δ13C
−47.0
−47.5
−48.0
BRW
NWR
MLO
[CH4]
1850
1800
1750
1700
1998
1999
YEAR

Figure 8

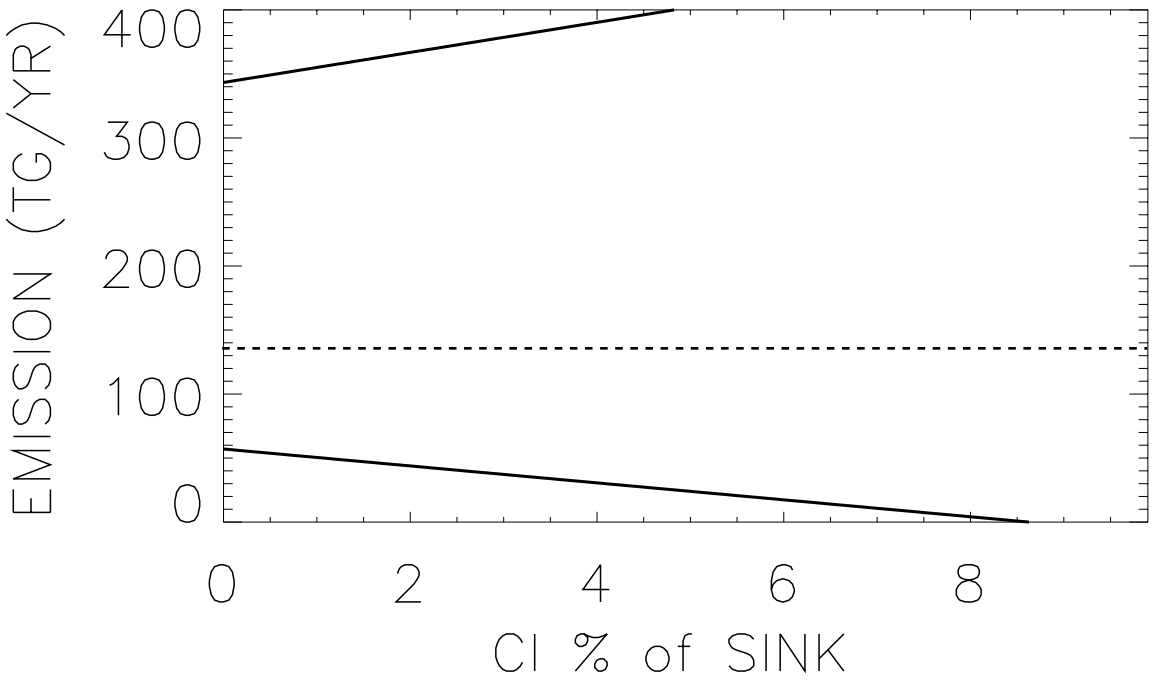

Figure 9

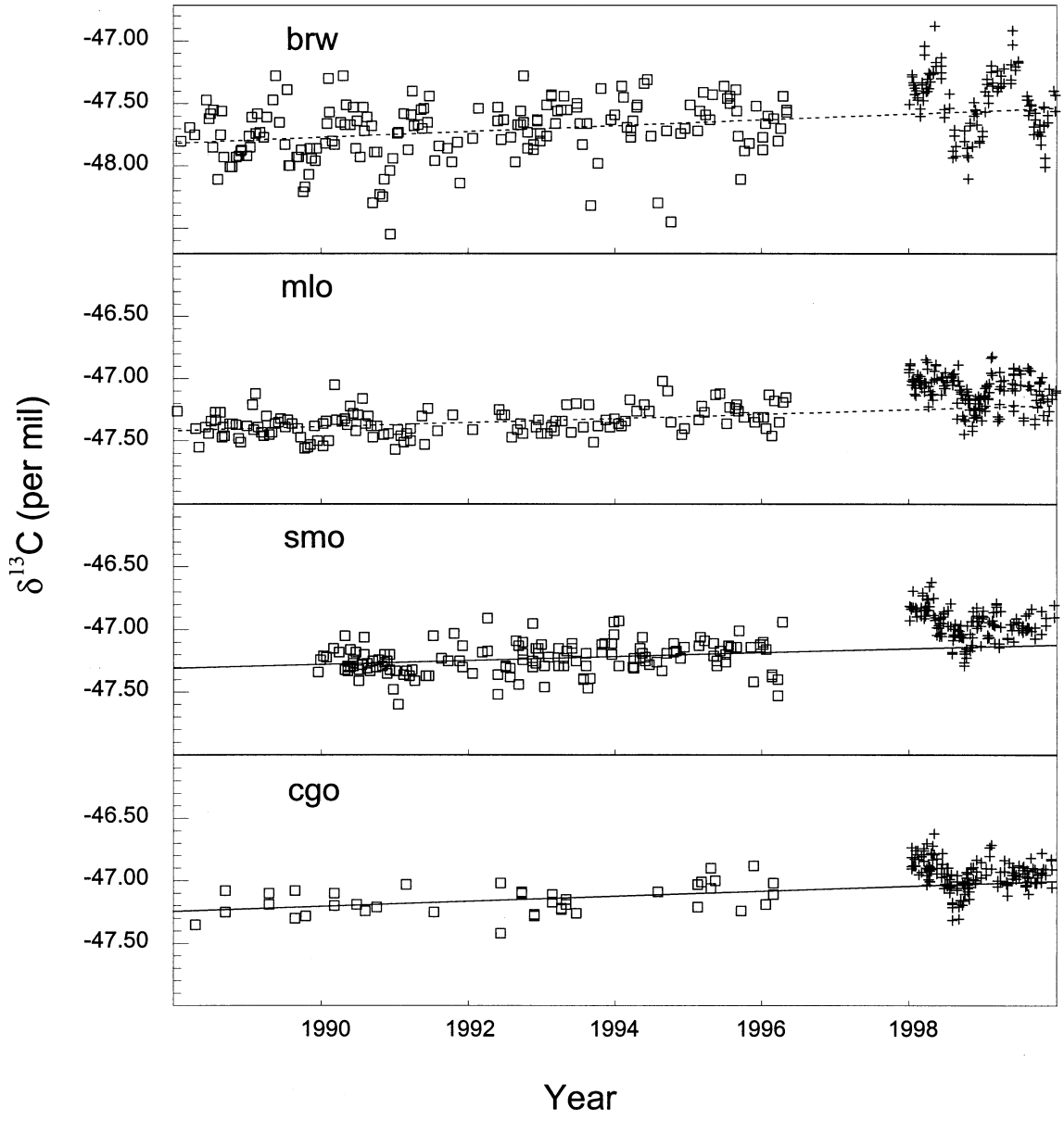
brw
mlo
smo
cgo
-47.00
-47.50
-48.00
-46.50
-47.00
-47.50
-46.50
-47.00
-47.50
-46.50
-47.00
-47.50
1990
1992
1994
1996
1998
Year
δ13C (per mil)

Figure 10

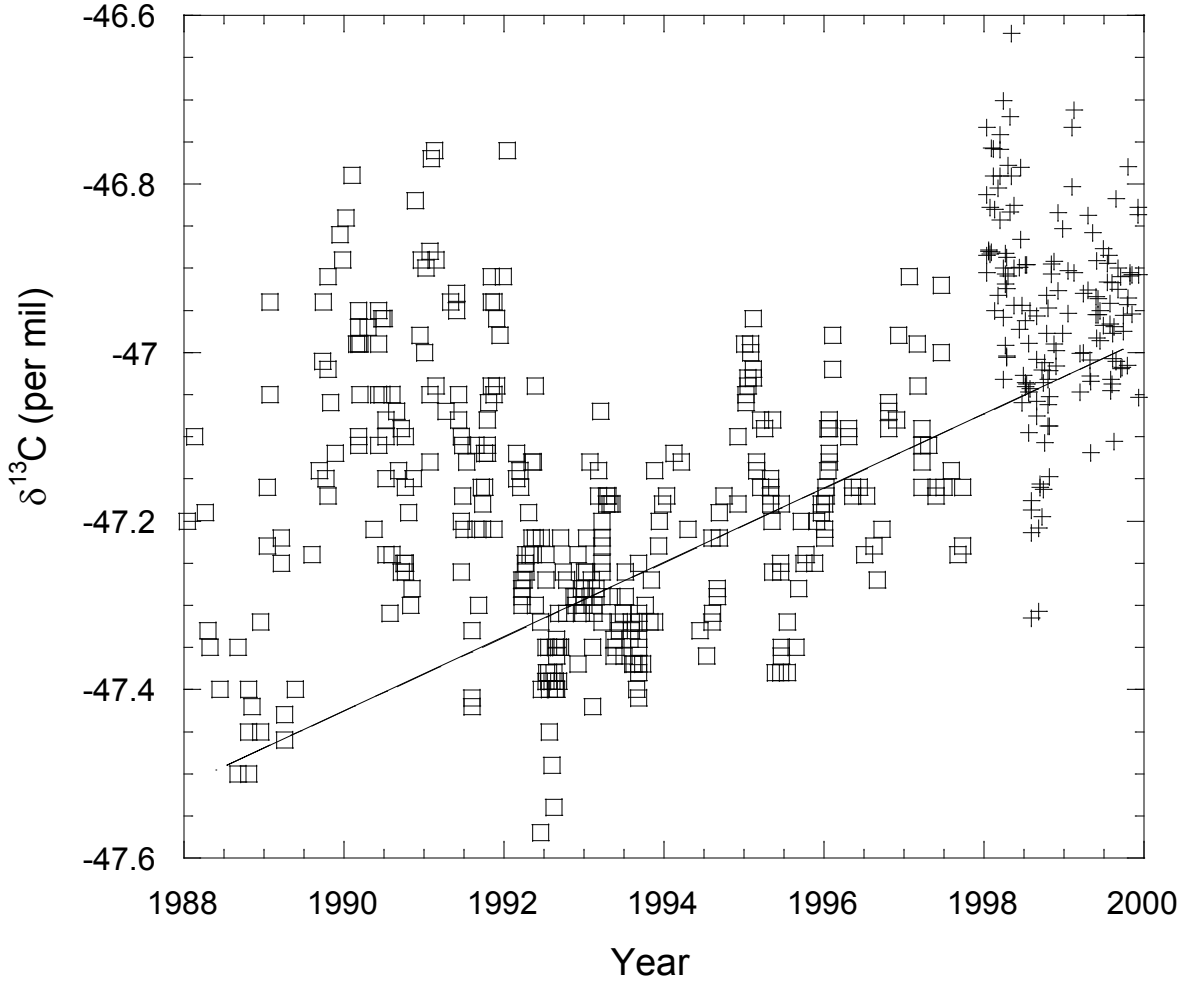
-46.6
-46.8
-47
-47.2
-47.4
-47.6
δ13C (per mil)
1988
1990
1992
1994
1996
1998
2000
Year

Figure 11